

## RESEARCH ARTICLE

10.1029/2021JD035570

## Key Points:

- Meso-Computing Atmospheric Trajectory model show dynamical connections between two sites of the western slope of Réunion Island
- Coupling of air masses with the Corine Land Cover—2018 register show that the origin of backward trajectories are biogenic area (3%–46%) and cultures areas (1%–17%)

## Supporting Information:

Supporting Information may be found in the online version of this article.

## Correspondence to:

M. Rocco and J.-L. Baray,  
manon.rocco@univ-reunion.fr;  
J.L.Baray@opgc.fr

## Citation:

Rocco, M., Baray, J.-L., Colomb, A., Borbon, A., Dominutti, P., Tulet, P., et al. (2022). High resolution dynamical analysis of volatile organic compounds (VOC) measurements during the BIO-MAÏDO field campaign (Réunion Island, Indian Ocean). *Journal of Geophysical Research: Atmospheres*, 127, e2021JD035570. <https://doi.org/10.1029/2021JD035570>

Received 15 JUL 2021

Accepted 16 JAN 2022

## Author Contributions:

**Conceptualization:** M. Rocco, J.-L. Baray, A. Colomb, P. Dominutti, N. Schoon

**Data curation:** M. Rocco, J.-L. Baray, A. Borbon, P. Tulet, C. Amelynck, N. Schoon, B. Verreyken, V. Duflot, V. Gros, R. Sarda-Estève, G. Péris, C. Guadagno, M. Leriche

**Formal analysis:** M. Rocco, A. Borbon, P. Dominutti, C. Amelynck










**Investigation:** M. Rocco, J.-L. Baray, A. Borbon, P. Dominutti, C. Amelynck, N. Schoon

**Methodology:** M. Rocco, J.-L. Baray

**Project Administration:** M. Rocco, M. Leriche

**Supervision:** M. Rocco, J.-L. Baray, A. Borbon

## High Resolution Dynamical Analysis of Volatile Organic Compounds (VOC) Measurements During the BIO-MAÏDO Field Campaign (Réunion Island, Indian Ocean)

M. Rocco<sup>1,2</sup> , J.-L. Baray<sup>1,3</sup> , A. Colomb<sup>1</sup>, A. Borbon<sup>1</sup> , P. Dominutti<sup>1,4</sup> , P. Tulet<sup>2,5</sup> , C. Amelynck<sup>6,7</sup>, N. Schoon<sup>6</sup>, B. Verreyken<sup>2,6,7,8</sup> , V. Duflot<sup>5</sup> , V. Gros<sup>9</sup> , R. Sarda-Estève<sup>9</sup>, G. Péris<sup>10</sup>, C. Guadagno<sup>10</sup>, and M. Leriche<sup>1,11</sup> 

<sup>1</sup>Laboratoire de Météorologie Physique (LaMP), Université Clermont Auvergne, CNRS, Clermont-Ferrand, France,

<sup>2</sup>Laboratoire de l'Atmosphère et des Cyclones (LACy), Université de la Réunion, CNRS, Saint-Denis, France, <sup>3</sup>Observatoire de Physique du Globe de Clermont Ferrand (OPGC), Université Clermont Auvergne, CNRS, Clermont-Ferrand, France,

<sup>4</sup>Institut des Géosciences de l'Environnement, Université Grenoble Alpes, CNRS, IRD (UMR 5001), Grenoble, France,

<sup>5</sup>Laboratoire d'Aérodynamique (LAERO), Université Paul Sabatier, CNRS, Toulouse, France, <sup>6</sup>Royal Belgian Institute for Space

Aeronomy (BIRA-IASB), Brussels, Belgium, <sup>7</sup>Department of chemistry, Ghent University, Ghent, Belgium, <sup>8</sup>Now at National

Oceanic and Atmospheric Administration (NOAA), Chemical Sciences Laboratory (CSL), Boulder, CO, USA, <sup>9</sup>Laboratoire des Sciences du Climat et de l'Environnement (LSCE), CNRS, Université Versailles Saint Quentin, Gif-sur-Yvette, France,

<sup>10</sup>ATMO-Réunion, Sainte-Marie, France, <sup>11</sup>Centre pour l'étude et la simulation du climat à l'échelle régionale (ESCE), Université du Québec à Montréal, Montréal, QC, Canada

**Abstract** This study presents a high-resolution dynamical analysis of Volatile Organic Compound (VOC) concentrations measured from March 11 to April 4 2019 at Réunion Island during the BIO-MAÏDO (Bio-physicochemistry of tropical clouds at Maïdo: processes and impacts on secondary organic aerosols formation) campaign. We detail the dynamical and chemical processes that govern atmospheric VOC concentrations at two targeted sites of the western slope of Réunion Island: Petite France (PF), 950 m above sea level (a.s.l.) and Maïdo Observatory (MO), 2150 m a.s.l. A dynamical connection between PF and MO is found during four selected days: March 28 and 31, April 1 and 3. Trajectory calculations using the coupling of Meso-Computing Advection-interpolation of atmospheric parameters and Trajectory tool (CAT) (100 m horizontal resolution of Meso-NH high-resolution non-hydrostatic model and the CAT trajectory model) Lagrangian transport model showed that air masses were dynamically linked between the two measurements sites for 19% of the time during the complete campaign. Trajectories from the Meso-CAT model combined with the Corine Land Cover-2018 register shows that backward-trajectories are frequently located above biogenic area (mixed forest, 3%–46% of total number trajectory point) and cultures area (e.g., sugar cane plantation, 1%–17%). Regarding VOCs concentrations, air masses coming from downhill MO are associated with significant measured concentrations of isoprene, isoprene oxidation products and benzene. Averaged concentration daytime ratios of isoprene and isoprene oxidation products from PF to MO are  $0.73 \pm 1.01$  and  $0.26 \pm 0.26$  respectively illustrating a loss of these VOCs due to deposition, oxidation, or possibility dilution on clouds.

### 1. Introduction

Volatile organic compounds (VOCs) in the atmosphere are fundamental in atmospheric chemical oxidation processes and are involved in health and climate impacts (Mellouki et al., 2015; Rumchev et al., 2007; Seinfeld & Pandis, 2016). VOC are emitted by both biogenic and anthropogenic sources and play an important role in atmospheric chemistry in ozone and secondary organic aerosol (SOA) formation (Ahern et al., 2019; Kesselmeier & Staudt, 1999; Sillman, 2002; Ylisirniö et al., 2020). The SOA can act as cloud condensation nuclei (CCN) leading to cloud formation (Andreae & Rosenfeld, 2008; VanReken et al., 2005) the climatic impact of which is not well known to date. A better understanding of the chemical processes governing the concentrations of these compounds is fundamental to improve air quality and climate modeling.

The campaign of the BIO-MAÏDO (Bio-physicochemistry of tropical clouds at Maïdo (2,150 m a.s.l.): processes and impacts on secondary organic aerosols formation) project took place in March–April 2019 at Réunion Island. The main objective of this project is to better understand the chemical and biological multiphase mechanisms that control SOA formation. Réunion Island is an ideal site for studying the formation of SOA and its role in cloud

**Validation:** A. Borbon, V. Duflot  
**Visualization:** M. Rocco, J.-L. Baray, P. Dominutti  
**Writing – original draft:** M. Rocco, J.-L. Baray, P. Dominutti, C. Amelynck, N. Schoon, V. Duflot  
**Writing – review & editing:** M. Rocco, J.-L. Baray, A. Colomb, A. Borbon, P. Dominutti, P. Tulet, C. Amelynck, N. Schoon, B. Verreyken, V. Duflot, V. Gros, M. Leriche

formation. Indeed, the island presents a tropical climate and strong slopes. Multiple studies detailed dynamic local circulations at Réunion Island (Foucart et al., 2018; Lesouëf et al., 2011, 2013). With high temperatures and strong sunlight, tropical climates favor the emission of biogenic VOCs (BVOCs) such as isoprene, and terpenes which may lead to the formation of SOA from low vapor pressure oxidation products (Rinne et al., 2002). Combined with the high-altitude difference conditions, air masses are cooling when they are advected with anabatic winds strengthened by the sea breeze phenomenon and play a large role in the formation of clouds. Furthermore, an increase in the height of the planetary boundary layer (PBL) is observed during the day (Garratt, 1992) which can bring VOC to the summit of the mountain. It was shown that clouds play a role in the variation of the altitude of the PBL and yield to a reduction of its altitude (Davis et al., 2020). Nighttime, the ground becomes cooler and air masses are going downhill (Monti et al., 2002).

The Maïdo observatory (MO) is an ideal place to perform coupled dynamical and chemical atmospheric studies in a tropical mountain island context (Baray et al., 2013). In 2015, a first field campaign (FARCE, forest–gas–aerosol cloud system, Duflot et al., 2019) took place with the goal to study interactions between the forest and the atmosphere. The analysis of measurements obtained, together with the use of the 3D non-hydrostatic high-resolution Meso-NH model (Lac et al., 2018; Lafore et al., 1998); showed that BVOCs are transported along the slope to the MO and play a large role in the formation of SOA. In the continuation of this study, the sources of formaldehyde have been characterized during the OCTAVE (oxygenated compounds in the tropical atmosphere: variability and exchanges) campaign in 2018 (Rocco et al., 2020). The impact of meso-scale transport features at Réunion Island has also been studied using an operational numerical weather prediction model, FLEXPART-AROME developed in the framework of the OCTAVE project (Verreyken et al., 2019). This model has then been used to qualify the impact of meso-scale transport toward MO to study biomass burning plumes, and to discuss temporal variations of VOC concentrations at the observatory (Verreyken et al., 2020, 2021).

The main objectives of the BIO-MAÏDO campaign are to characterize the atmospheric dynamic processes and cloud formation along the slope of the MO, to characterize the chemical composition of the air masses and cloud water, to identify chemical sources, and to determine case studies for 0D and 3D modeling. The set up during the BIO-MAÏDO campaign consisted of five measurement sites at different altitudes (Petite France (PF), 950 m a.s.l.; Domaine des Orchidées Sauvages, 1,250 m a.s.l.; Maïdo hostel, 1,400 m a.s.l.; Piste Oméga, 1,750 m a.s.l. and the MO, 2,150 m a.s.l.) with the purpose to measure a comprehensive data set of chemical, physical and biological variables in the atmosphere (<https://lacy.univ-reunion.fr/activites/programmes-de-recherche/bio>, last accessed on November 10, 2021). The present study is part of the chemical characterization of air masses and chemical sources identification.

To fulfill these objectives, the concentrations of VOCs obtained during the BIO-MAÏDO campaign are analyzed by proton-transfer-reaction mass-spectrometry (PTR-MS) instruments in two of the five measurement sites: PF (950 m a.s.l.) and the MO (2,150 m a.s.l.) and linked to trajectories of Meso-CAT (Computing Advection-interpolation of atmospheric parameters and Trajectory tool) model, which is the coupling of Meso-NH and CAT (new version of the lagrangian LACYTRAJ model; Clain et al., 2010) models in various spatial domains having different sizes and resolutions (Figure 1). The objective of this study is to explain the variations of VOC concentrations at the two selected sites by characterizing the atmospheric dynamics and the Land Cover Footprint obtained by coupling high resolution forward and backward trajectories and the Corine Land Cover register (Géoportail, <https://www.geoportail.gouv.fr/>, last accessed on November 10, 2021). In the first part of this article, material and methods are presented including the characteristics of Meso-CAT. In the second part, we present a coupled chemical-dynamical analysis of the campaign, focusing on four selected days: March 28 and 31, and April 1 and 3, when the two sites present a dynamical connection according to the Meso-CAT simulations.

## 2. Materials and Methods

On-line VOC measurements have been performed from March 11, to April 4, 2019 at PF specifically for BIO-MAÏDO. These measurements complement the 2-year long-term measurements performed at MO between October 2017 and November 2019 in the framework of the OCTAVE project (Verreyken et al., 2021). Meso-NH simulations were used to calculate high resolution backward and forward trajectories with the Meso-CAT model on the period from March 26, to April 6. We provide a short description of the instrumental set-up, which is

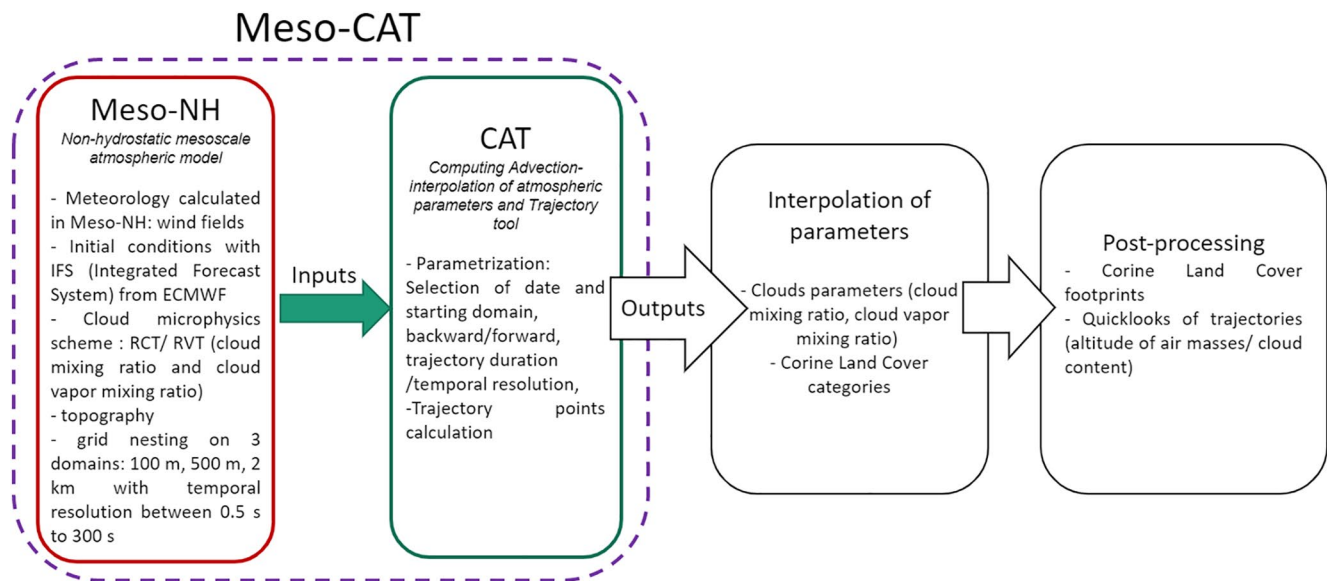


**Figure 1.** Flowchart of Meso-Computing Advection-interpolation of atmospheric parameters and Trajectory tool (CAT) model resulting from the coupling of Meso-NH and CAT models.

similar to the one deployed during the OCTAVE campaign (<https://octave.aeronomie.be/index.php>, last accessed on November 10, 2021), and has been described elsewhere (Rocco et al., 2020; Verreyken et al., 2021).

### 2.1. Sampling Sites of VOCs

PF is a rural village of 4,000 inhabitants located west of Saint Paul, urban area of almost 100,000 inhabitants (2018, INSEE), at almost the top of the mixing boundary layer (MBL) during the night and in the MBL during the day. The mobile laboratory was installed near a meadow uphill from the village alongside the road toward Maïdo. MO is a remote altitude site located in a convergence layer of two distinct regimes: local upslope and downslope winds resulting in thermodynamic processes and complex and variable local air circulation patterns.

Réunion Island is located in a region with strong south-easterly winds. The island represents a great obstacle due to its steep topography and high elevation of the mountains (Piton des Neiges, 3,070 m a.s.l.; Piton de la Fournaise, 2,632 m a.s.l.). The trade winds facing the South-Eastern part of the island are separated into two flows along the coast of the island and are accelerated (Venturi effect), while in the north-west side of the island, there is a recirculating flow called “return flow” or counter-flow (Lesouëf et al., 2011). During the daytime, the heating of the surface by solar radiation induces upward transport of air masses along the island surface (anabatic winds) which are coupled with the sea-breeze phenomenon. Upslope transport cooled down the air due to the change in altitude. This forced cooling leads to the formation of clouds on a near-daily basis. During the night, the phenomenon reverses and katabatic winds and land breeze processes become prevalent (Davis et al., 2020; Garratt, 1992; Monti et al., 2002). During the daytime, MO is mostly located in the PBL while at night, air masses arriving at the observatory originate mostly from the free troposphere.

The meteorological parameters (temperature, humidity, pressure...) have been measured at the two sites. Wind speed and direction have been measured in both sites using a Vaisala sensor (Vaisala, Helsinki, Finland, <https://www.vaisala.com/>, last accessed on November 2, 2021). The meteorological parameters have been recorded by an automatic weather system (AWS).

### 2.2. Meso-CAT: A Coupling of Meso-NH and CAT Models

CAT (Baray et al., 2020), is an atmospheric tracer trajectory/advection/interpolation tool, which allows the calculation of a large number of trajectories, using the global analysis ECMWF product ERA-5 coupled with topography matrices on 2 arc min resolution grid (Bezděk & Sebera, 2013). CAT has already been used to determine

statistics of air masses arriving at the Puy de Dôme observatory (Baray et al., 2020) and to classify clouds in association with chemical measurements in cloud water (Renard et al., 2020).

Meso-NH is a non-hydrostatic mesoscale atmospheric model, which has been jointly developed by Laboratoire d'Aérodynamique (LAERO, UMR 5560 UPS/CNRS) and Centre National de Recherches Météorologiques (CNRM, UMR 3589 CNRS/Météo-France; Lac et al., 2018; <http://mesonh.aero.obs-mip.fr/mesonh54/Welcome>, last accessed on November 2, 2021). Meso-NH simulates small scale (Large-Eddy Simulations (LES) type, horizontal resolution of a few meters) to synoptic-scale atmospheric parameters (horizontal resolution of several tens of kilometres) and can be run in a two-way nested mode involving up to eight nesting stages. Surface fluxes are computed by a coupling between Meso-NH and the surface model SURFEX (Masson et al., 2003). Several parameterisations of cloud microphysics are available in Meso-NH. In this study, the ICE-3 module is used (Lac et al., 2018; Lafore et al., 1998; Pinty & Jabouille, 1998). The Meso-NH model has already been used to characterize air masses above Réunion Island at 500 m resolution during the FARCE campaign (Duflo et al., 2019).

The Meso-NH configuration used in the present work includes three nested domains at the horizontal resolutions 100, 500, and 2,000 m (Figure 1). The small domain (100 m resolution) covers only a small area of about 5 km around the measurement sites. The two largest domains (500 m and 2 km resolution) cover the entire island. The initial and boundary conditions for meteorology were provided by the AROME operational high-resolution analysis with a horizontal and temporal resolution of 2.5 km and 6 hr, respectively.

All three domains include 72 vertical points, with a vertical stretched resolution decreasing with height, from a few meters (near the ground level) up to 1 km (from 8 km above sea level to the top of the domain). The temporal resolution of the model for the three domains ranges between 0.5 and 300 s depending on their size.

For this work, we developed Meso-CAT, a new version of CAT, which assimilates high-resolution atmospheric parameters and topography from Meso-NH outputs to compute forward and backward trajectories (Figure 1).

Two types of trajectories are computed: the first makes use of the domain at 100 m resolution documenting the very local dynamical connection between the measurement sites, and the second is based on the domain at 500 m resolution documenting the dynamics of air masses at a larger scale.

All trajectory sets consist of trajectories, distributed in a cube around the measurement site. The dimensions of the starting domain are about 500 m (or 100 m for precision plots) horizontally and 50 m vertically above ground level. Trajectory points have been calculated with a temporal resolution of 5 min (interval for which the position of a parcel is computed) for 12 hr. This time resolution has been estimated as the best compromise to study the origins of air masses. In (Verreyken et al., 2021), FLEXPART-AROME simulations show near identical contributions from island emissions between 12 and 24hr back trajectories. This implies that FLEXPART-AROME suggest that the effect of local emissions is negligible after 12hr of transport.

Humidity and cloud mixing ratios (kg/kg) have been interpolated on all Meso-CAT trajectory points.

Land cover footprint (industrial, oceanic, biogenic or urban) is estimated by interpolating the type of ground surface below each trajectory point obtained from the Corine Land Cover-2018 data (Geoportail, <https://www.geoportail.gouv.fr/>, last accessed on November 10, 2021). The register spatial resolution is around 70 m. The calculation of the relative land cover footprint is based on trajectory points located below 500 m above ground level since air masses located above this altitude are not very sensitive to surface emissions. This threshold has already been used in Dominutti et al. (2021). Figure 2 shows the Corine Land Cover-2018 map and land use categories detailed in the register.

In this study, the categories are grouped into five classes and used to analyze the origins of air masses: oceanic, anthropogenic, cultures, natural vegetation, and others. The “other” category comprises land cover such as bare rocks, estuaries, beaches, or inland marshes. The anthropogenic category groups traffic, urban, industrial and harbor areas. Trajectory points located above 500 m are classified in a sixth “upper altitude” category which corresponds to points which are considered to be not sensitive to surface emissions. After this interpolation, a percentage of trajectory points associated with the categories is calculated for each trajectory set.

Figure 3 shows 12 hr Meso-CAT backward trajectories compared with FLEXPART-AROME (initialized with AROME at 2.5 km horizontal resolution [Verreyken et al., 2019]) and HYSPLIT (user-friendly model to compute air parcel trajectories, here initialized with GDAS at 1° resolution and GFSG at 0.5° resolution,

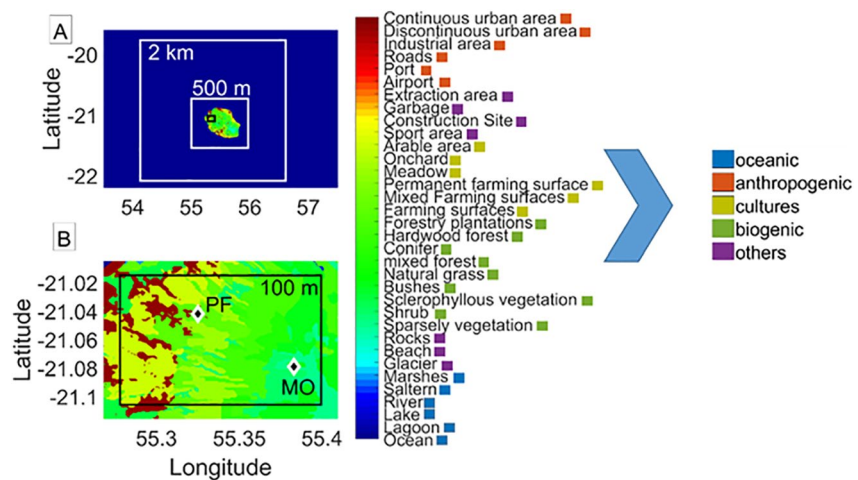


**Figure 2.** (a) Corine Land Cover-2018 map of Réunion island. The colormap is based on the Corine category numbers and the white rectangles show the limits of the Meso-NH domains. All categories are grouped in oceanic, anthropogenic, cultures, biogenic and others categories. (b) Location of the measurement sites: Petite France (PF, 950 m a.s.l.) and Maïdo Observatory (MO, 2,150 m a.s.l.). The black rectangle indicates the limits of the high resolution (100 m) Meso-NH domain.

[https://www.ready.noaa.gov/HYSPLIT\\_traj.php](https://www.ready.noaa.gov/HYSPLIT_traj.php), last accessed on November 2, 2021 [Rolph et al., 2017; Stein et al., 2015]), for March 30 at 19hr UT. For this example both FLEXPART-AROME backward trajectories (total column and footprint 0–1 km above ground level Figures 3c and 3d) agree well with Meso-CAT at 500 m spatial resolution (Figure 3a). The local counter flow (air masses advected from northwest of the island, see Section 2.1.) is well reproduced by the two models. The FLEXPART-AROME backward trajectory for the total column is almost identical to the one with the footprint between 0 and 1 km indicating that almost all the trajectories are close to the ground. In contrast, Meso-CAT shows some trajectories above 3 km. This difference could be due to the different resolutions of the wind field (500 m vs. 2.5 km). HYSPLIT (Figure 3e) presents a different large-scale origin of air masses depending on meteorological data used. Unsurprisingly, because of the low resolution of GDAS, the local dynamical circulations cannot be simulated with HYSPLIT whatever the resolution of wind data. The fact that the starting altitude of the HYSPLIT trajectories is 2,150 m above ground level with GDAS at 1° and 1,719 m with GFSG at 0.5° implies that, given the spatial resolution of wind input data, the MO (2,150 m a.s.l.) corresponds to a point of the grid at the sea level at 1° and at 656 m above sea level at 0.5°. Furthermore, the origin of the wind is not the same at 0.5° and 1° increasing the uncertainty on the wind origin of these trajectories. This implies that HYSPLIT with GFSG at 0.5° and GDAS at 1° cannot be used to study the variation of winds at small scales. These comparisons show that Meso-CAT is useful to study air masses at a small scale, using a 500 m horizontal resolution to cover the entire island, and at very small scale in a 100 m resolution domain very close to the measurement point.

### 2.3. Online Measurements of VOCs by PTR-MS: Proton-Transfer-Reaction Mass-Spectrometry

Proton-transfer-reaction mass-spectrometry is a well-known technique used for measuring in-situ VOC concentrations (Blake et al., 2009; Lindinger et al., 1998). The technique is based on the proton transfer reaction of  $H_3O^+$  ions with VOCs in the drift tube reactor of the instrument, resulting in the protonated VOC for VOCs with a proton affinity higher than the one of water vapor. Primary and product ions are mass-separated in a quadrupole mass spectrometer before being detected by a secondary electron multiplier. VOC mixing ratios are obtained by dividing the background-subtracted ion signals by the corresponding calibration coefficients. Data from two high-sensitivity PTR-MS instruments (hs-PTR-MS, Ionicon Analytik GmbH, Innsbruck) were used for the present study. One of them was located at MO and deployed by the Royal Belgian Institute for Space Aeronomy (BIRA-IASB) to provide a long-term series of VOC measurements in the framework of the OCTAVE project (<https://octave.aeronomie.be/index.php>). The other PTR-MS instrument was located at PF and provided by the Laboratoire des Sciences, du Climat et de l'Environnement (LSCE).

The methodology for both PTR-MS instruments has been explained and detailed in the following subsections:

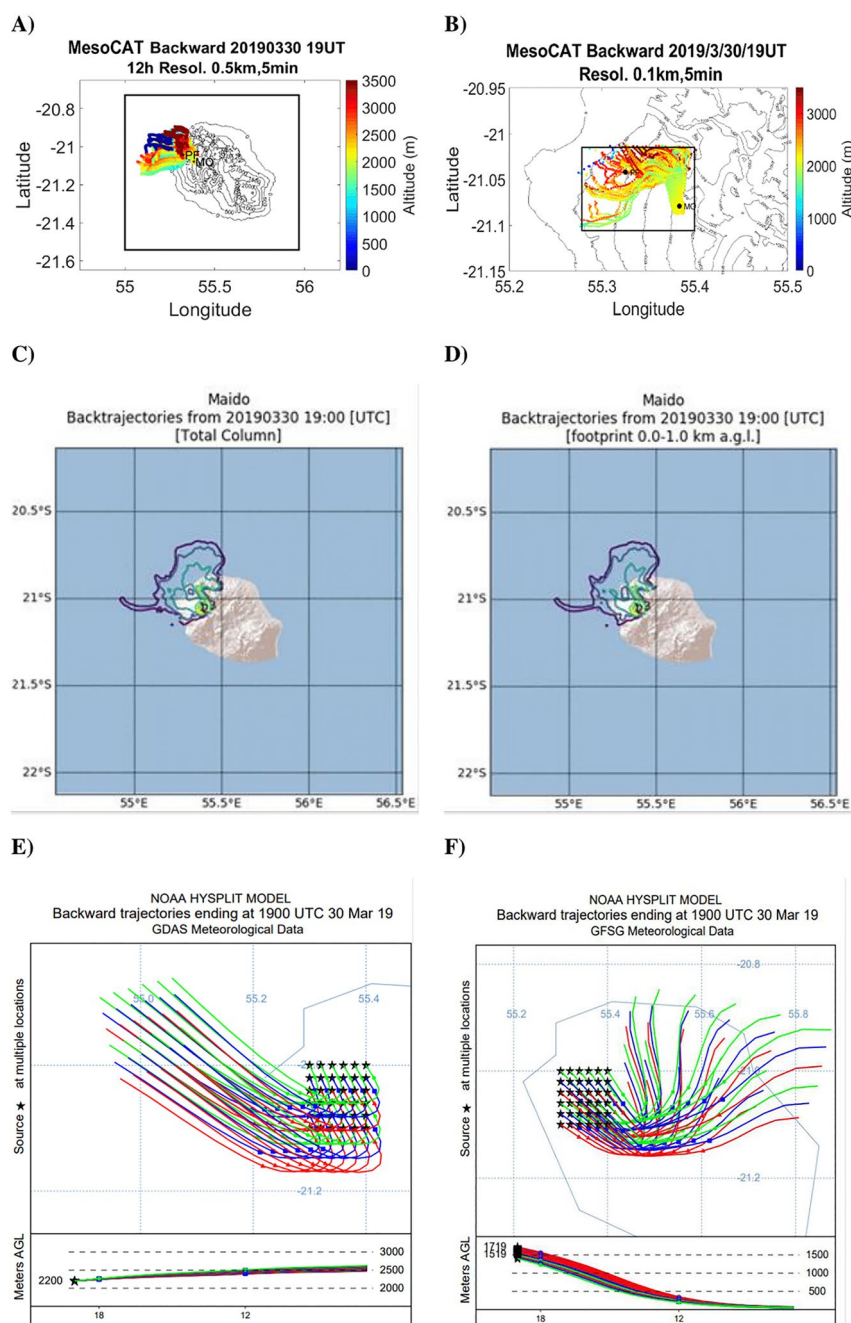


**Figure 3.** Backward trajectories from the Maïdo observatory computed with (a) Meso-Computing Advection-interpolation of atmospheric parameters and Trajectory tool (Meso-CAT) at 500 m spatial resolution, (b) Meso-CAT at 100 m spatial resolution (c) FLEXPART-AROME at 2.5 km horizontal resolution and considering total column (d) FLEXPART-AROME at 2.5 km horizontal resolution and considering 0–1 km above the ground level and (e) Hysplit with GDAS at 1° and (f) Hysplit with GFSG at 0.5°.

### 2.3.1. BIRA PTR-MS

The following VOCs species were measured continuously by the BIRA PTR-MS: formaldehyde (m/z 31) methanol (m/z 33), acetonitrile (m/z 42), acetaldehyde (m/z 45), formic acid (m/z 47), acetone (m/z 59), acetic acid (m/z 61), dimethyl sulfide (DMS, m/z 63), isoprene (m/z 69), isoprene oxidation products (m/z 71), benzene (m/z 79), toluene (m/z 93), C8-aromatics (m/z 107), and the sum of monoterpenes (at m/z 81 and m/z 137) with a dwell time of 10 s. Calibrations were performed every 3–4 days with a custom-made calibration unit using an

ApelRiemer VOC calibration mixture (ApelRiemer Environmental Inc.). Besides the above listed compounds, the calibration bottle contained methyl vinyl ketone (MVK) and methacrolein (MACR) as isoprene oxidation products and limonene to represent the family of monoterpenes. Formic and acetic acid, which were not present in the calibration bottle, were quantified based on first principles and data from the literature (Baasandorj et al., 2015; Verreyken et al., 2021).

During the period of interest, a calibration versus relative humidity was performed on April 2, 2019 by controlling the humidity of the zero air, in which the calibration gas was diluted, with a dew point generator (LI-COR LI-610, NE). The ion signal at  $m/z$  37 was used as a proxy for air humidity. More details are provided in Verreyken et al. (2021). Detection limits (DL) were calculated as three times the standard deviation of the background signals, divided by the calibration factors. The precision of the individual 10 s measurements for the different compounds was obtained by taking into account Poisson statistics for the source and product ion counts, as well as statistical errors related to the interpolation of less frequent (every 4 hr) background measurements and calibration factors (every 3–4 days), and the precision of the calibration factors themselves. The error on the compound mixing ratio in the calibration bottle (5% at the  $2\sigma$  level) and the error on the dilution factor of the calibration gas in zero air (1.9%) were considered to determine the systematic error on the mixing ratios.

### 2.3.2. LSCE PTR-MS

For the LSCE PTR-MS, selected VOC species were methanol ( $m/z$  33), acetonitrile ( $m/z$  42), acetaldehyde ( $m/z$  45), acetone ( $m/z$  59), isoprene ( $m/z$  69), isoprene oxidation products ( $m/z$  71), benzene ( $m/z$  79), toluene ( $m/z$  93), C8-aromatics ( $m/z$  107), and monoterpenes ( $m/z$  137) with a dwell time of 5 s per VOC-related mass. Blank measurements were performed every 8 hr. The LSCE PTR-MS was calibrated with a commercial Calibration Gas Unit (Ionicon Analytik GmbH, Innsbruck). This GCU contained an Ionicon VOC mixture containing all monitored VOCs, with the exception of isoprene oxidation products. Calibrations have been performed before and at the end of the campaign. Calibration coefficients from the first calibration have been used to calculate VOC concentration from the start of the campaign to March 21 and the second set of calibration coefficients have been used from March 22 until the end of the campaign. The choice of these two periods have been made because of the re-start of the PTR-MS on March 22 after a measurement interruption due to an electrical power shutdown on March 21. The relative difference between these two calibrations is 11.9%, 2.9%, 2.0%, 8.4%, and 3.8% for methanol, acetaldehyde, acetone, isoprene and benzene, respectively. The influence of humidity was not considered in the calibration, as this instrument was shown to present very similar results with dry and humidified air (Holzinger et al., 2019). Nevertheless, as the calibrations were performed with a standard diluted with ambient (and therefore humid) air, the derived calibration coefficients were representative of local humidity conditions. Error calculations on the mixing ratios were performed in a similar way as for the BIRA PTR-MS.

### 2.3.3. Intercomparison of Both PTR-MS

In this study, we focus on five compounds: methanol, acetone, isoprene and its oxidation products and benzene. Their DL, systematic error, precision and combined uncertainty are presented in Table 1. Concentrations of toluene, monoterpenes, and C8-aromatics are not considered due to very large background values which generates a lot of concentrations values under the detection limit. As observed acetonitrile concentrations are quite low at the MO and this compound is mostly emitted during biomass burning events (occurring from August to November and not during March–April; Verreyken et al., 2021; Vigouroux et al., 2012), we chose to not include this compound in our set of data for studying the local origin of air masses. Concentrations below the DL were set to half of DL for the normalized concentration of nighttime values (see Section 3.3).

These two instruments have already participated in a measurement campaign at Réunion Island in 2018, where they have both been calibrated against the two calibration units (the home-made BIRA-IASB unit containing an ApelRiemer standard and the commercial GCU unit containing an Ionicon standard). A good agreement (coefficient of determination  $R^2$  higher than 0.90) for the common compounds in the mixtures was found and this was repeated with the BIRA-IASB PTR-MS prior to the start of the BIO-MAÏDO campaign (March 9, 2019). In order to assure comparability of VOC measurements with the two PTR-MS instruments. The relative differences between the calibration coefficients obtained with the two calibration units were  $-17\%$ ,  $-6\%$ ,  $5\%$ ,  $36\%$ , and  $2\%$  for methanol, acetone, isoprene,  $m/z$  71, and benzene, respectively. The large relative difference observed for methanol was due to the relatively short duration of the calibration with the Ionicon GCU during which methanol concentrations did not reach an equilibrium. A large discrepancy was found between the calibrations factors at

**Table 1**  
Summary Table of Detection Limits (LD) in ppb, and Median Relative Accuracy, Precision and Uncertainty (in %) of the Compound Mixing Ratios During the Campaign

Compound	PTR-MS	DL (ppb)	Systematic error	Precision	Combined uncertainty
Isoprene	BIRA	0.021	3.1%	12%	13%
	LSCE	0.048	5.6%	22%	23%
Isoprene oxidation products	BIRA	0.009	3.1%	9.6%	10%
	LSCE	0.052	5.6%	25%	26%
Methanol	BIRA	0.170	3.1%	8.0%	8.6%
	LSCE	0.213	5.6%	27%	28%
Acetone	BIRA	0.022	3.1%	3.7%	4.9%
	LSCE	0.057	5.6%	8.6%	10%
Benzene	BIRA	0.009	3.1%	35%	36%
	LSCE	0.021	5.6%	42%	43%

*Note.* Whereas the precision reflects the random error on the measurements obtained by applying counting statistics, the systematic error includes errors on the VOC mixing ratios in the standard and on the dilution of the calibration gas in the calibration unit. The total combined uncertainty ( $1\sigma$ ) is given by  $\sqrt{\text{precision}^2 + \text{systematic error}^2}$ .

m/z 71 with the two calibration systems because the ApelRiemer calibration mixture in the BIRA-IASB set-up contained MACR and MVK whereas the LSCE calibration system contained crotonaldehyde. A correction factor of 1.364 (calibration factor of crotonaldehyde/calibration factor of MVK/MACR as determined from this experiment) was therefore applied to the concentrations of m/z 71 compounds obtained with the LSCE PTR-MS which was calibrated with the Ionicon GCU unit during the entire BIO-MAÏDO campaign, to be able to compare concentrations of isoprene oxidation products at both sites.

More details about the instrumental set up can be found in Rocco et al. (2020) and Verreyken et al. (2021).

### 3. Chemical Context and Emission Sources

#### 3.1. Dynamical Connection Between the Two Sampling Sites and a Case Study Selection

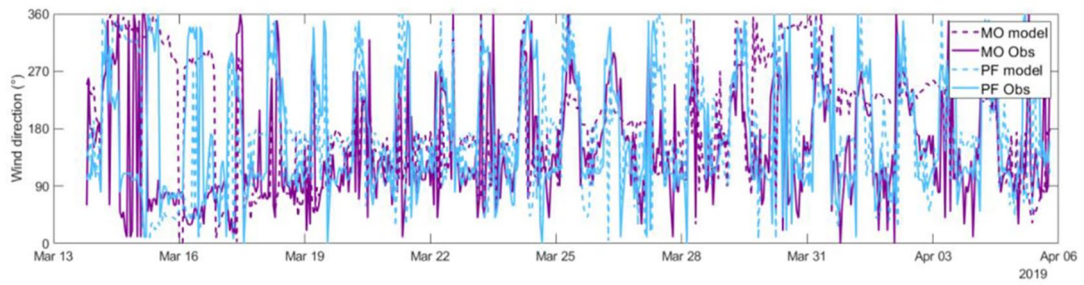
Comparison of observed and computed wind direction and wind speed are shown in Figures 4a and 4b. Wind speed and direction observations are based on Météo France data stations very close to PF and MO BIO-MAÏDO sites and Meso-NH points are the closest points from MO and PF sites in the 100 m resolution domain (for a better comparison). Figure 4a shows a good agreement between observed and computed wind directions at PF and MO. Topography effects (steep mountain slopes around MO for example) can explain some discrepancies in wind speed and direction between model and observations especially for MO which is near steep slopes.

To properly interpret the VOC measurements performed at PF and MO, it is useful to establish whether the sites were dynamically connected, that is, if an air mass corresponding to a measurement on one site has been advected to (or is coming from) the other site. For this, the dynamical connections have been estimated by compiling forward and backward trajectory calculations in the 100 and 500 m resolution domains. We consider that a dynamical connection exists between the two sites if a part of the cluster of trajectories at one site approaches the other within  $0.02^\circ$  (about 2 km which is a good compromise with the spatial resolution of the wind fields) in at least one of the two domains and less than 1 km above the ground. On average, from March 15 to April 6, up to 1.5% of trajectory points are reaching the other site.

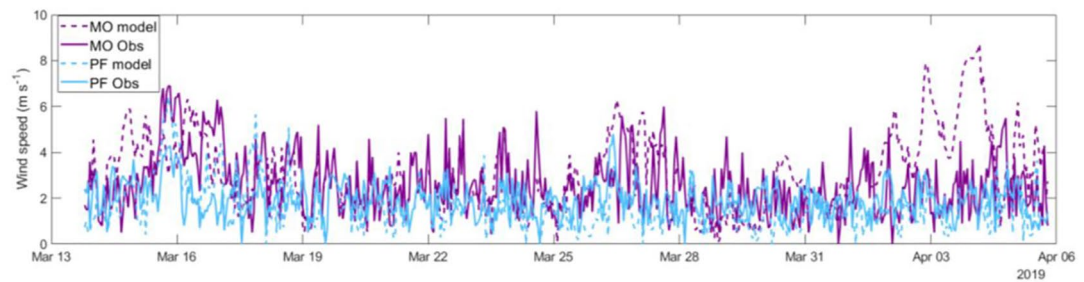
The occurrences of dynamical connection have been calculated every 15 min from March 15 to April 6 on the base of forward (PF to MO) and backward (MO from PF) trajectories (Figure 4c). During this period and when measurements of VOC were in operation in both sites, 6 days show a more pronounced dynamical connection occurrence between PF and MO: March 15, 16, 28, 30, and 31 and April 1. This study focuses now on March 28 and 31 and April 1 and 3.



A



B



C

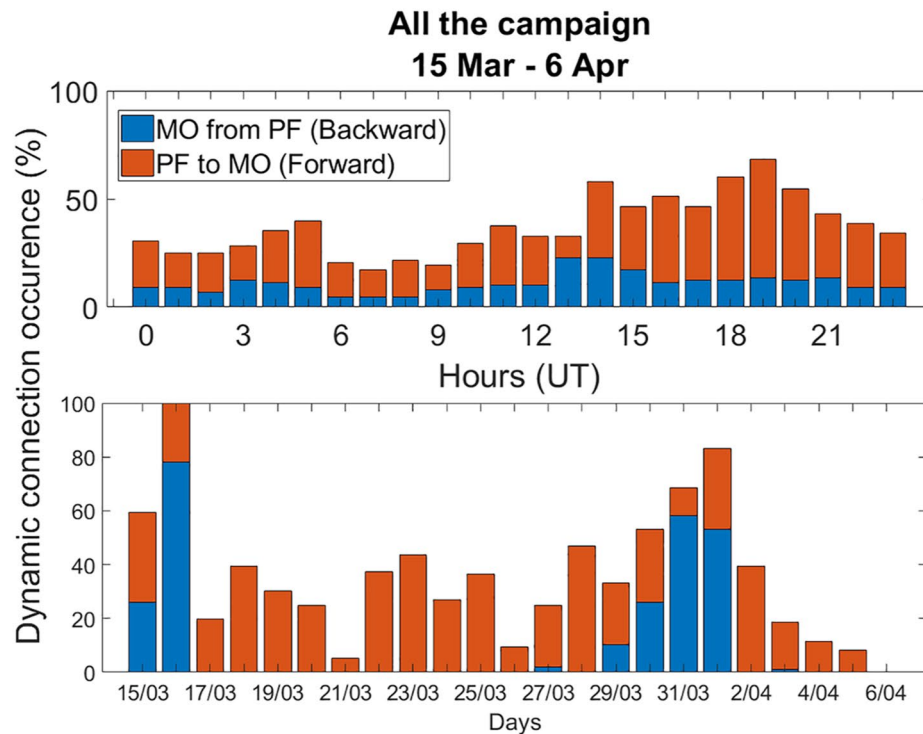


Figure 4.

**Table 2**  
Summary Table for Dynamical Connection Percentages for the Four Selected Days and From March 15 to April 6

Date (DD/MM/YYYY)	% Of dynamical connection calculated with backward trajectories (MO from PF)	% Of dynamical connection calculated with forward trajectories (PF to MO)	% Of total dynamical connection (all trajectories)
28/03/2019	0	58	58
31/03/2019	58	13	13
01/04/2019	53	29	28
03/04/2019	1	21	21
15/03 to 06/04/2019	13	26	19

The forward and backward connections can be different due to time shifts between the forward and backward trajectories and because of the height differences between the starting and the target volumes (for PF: 1,000–2,000 m a.s.l. and MO: 2,150–3,200 m a.s.l.). As is shown in Figure 4c (top), the average daily variation reveals that more connections are occurring from 10hr UT to 23 hr UT (local time = UT + 4 hr). Some connections are observed during the night (from PF reaching MO), but the maximal occurrence of connections (more than 50%) is obtained during the afternoon, when the anabatic winds and sea breezes are occurring. Figure 4c (bottom) presents the time-series of daily connections from 15 March to 6 April. The maximum percentage of connections is observed from March 15 to 16 and from March 28 to April 1, reaching at least 82%. The highest dynamical connection percentage is observed on April 1. A lower percentage of connection is observed on March 21 and 26, April 4 and 5 for example, and could be related to the high altitude of most of the trajectory points.

Maxima of connections have been observed for the four selected days for both backward and forward trajectories (see Table 2). Globally, the percentage of dynamical connection between the two sites (considering all days, hours and directions) is 19% (Table 2).

The wind direction measured locally is not always well linked with the larger scale pattern found for the trajectory's connection which depends on the three-dimensional wind patterns, nevertheless this is generally the case during BIO-MAÏDO campaign (Figure 5). Daytime, wind direction (4–14 hr UT) is mainly from north and west in MO and PF, the change of wind is observed markedly by few connections between the two sites. At 4 hr UT (sunrise), the surface starts heating by absorption of solar radiation, the wind direction changes at PF and comes from the west. Anabatic and sea breeze processes occur, and the air is advected uphill to MO. At 7 hr UT, the wind regime changes at MO (wind from the north). Between 7 and 10 hr UT, air masses from PF to MO are less connected and show an only connection for forward trajectories at 8 and 10 hr UT. This change is complex to explain but this period matches with the cloud formation (Lesouëf et al., 2013) and, therefore, the circulation of air masses changes under cloudy conditions. Moreover, clouds change the radiation and limit the heating of the ground that can reverse the thermal processes (anabatic winds and sea breeze). Nevertheless, we observed a predominance of subsiding air masses which explains the link between the two sites from 10 to 14 hr UT.

The main nighttime wind direction is ENE at PF and ESE at MO (Figure 5) and it presents the greatest connection between the two sites. Air masses come from the South-East of the island, reach MO and go down to PF (e.g., with backward trajectories in PF, in Figure S1 in Supporting Information S1). Winds at PF are in the same order of magnitude for day and night (average wind of  $2.37 \pm 0.69$  m/s during the day and  $2.94 \pm 0.51$  m/s during the night) but are more variable at MO, especially during the night (average wind of  $1.78 \pm 0.95$  m/s during the day and  $2.71 \pm 1.31$  m/s during the night). Lesouëf et al. (2011) showed that when air masses come from NE with weak wind speed, a “cap” effect cannot be observed, and the air masses pass over MO. The “cap” effect is occurring if the latter is sufficiently weak and allow the development of breezes on the west coast, air pumping from lower layers protects the mountains from NE winds, forced to pass over a “cap”. In contrast, when winds have high intensity, air masses pass over MO and can more easily go down to PF. Since the 100 m trajectories domain is too small to include the whole circulation patterns at the scale of the island, calculations on the 500 m domain are used to provide a better estimation of the main land cover footprint sources (anthropogenic and/or biogenic) leading to the VOC concentrations at MO (Section 3.2.3).

**Figure 4.** (a) Time series comparison of observed and computed wind direction (°) from March 15 to April 6, 2019 at Maïdo observatory (MO) and Petite France (PF). (b) Time series comparison of observed and computed wind speed ( $\text{m s}^{-1}$ ) from March 15 to April 6, 2019 at MO and PF. The solid blue line and purple line represent observed wind direction or speed at PF and MO, respectively. Blue and purple dots: computed wind direction or speed at PF and MO, respectively. (c) Dynamic connection occurrence (%) from March 26 to April 6 considering both 500 and 100 m domains with 15-min time resolution trajectories. Top: Daily variation of dynamic connection occurrence from 0hr UT to 23 hr UT. Bottom: Dynamic connection occurrence for each day.

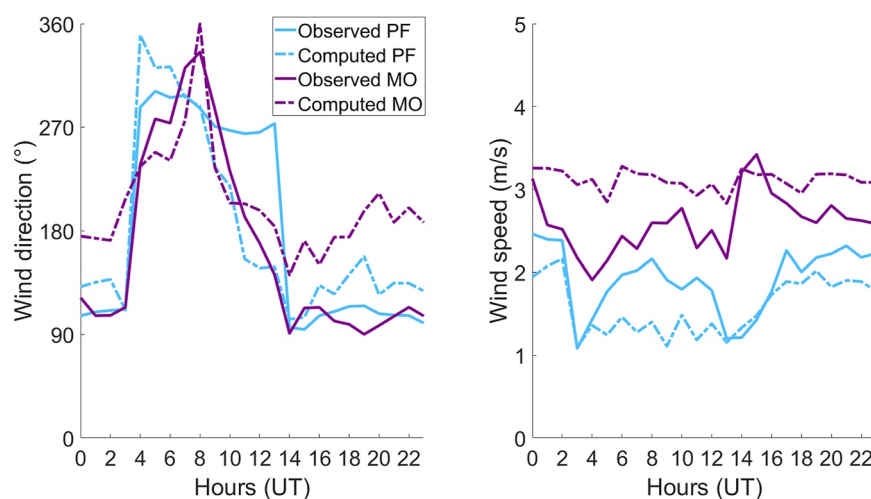


**Figure 5.** Comparison of daily variation of observed and computed wind speed ( $\text{m s}^{-1}$ ) and wind direction ( $^{\circ}$ ) at Maïdo observatory and Petite France (averaged over the entire campaign).

### 3.2. Variability of VOCs Concentrations and Ratios

Diurnal variation of methanol, acetone, benzene, isoprene and its oxidation product concentrations are represented in Figure 6 for the four selected days. Day and night concentrations and isoprene oxidation product on isoprene concentration ( $\sigma$ ) are listed in Table 3. For all compounds, residuals concentrations of VOCs can be observed during the night at PF that it is not observed at MO for short lived-compounds (isoprene and its oxidation products and benzene). This fact could be related to the boundary conditions at MO during the night, in general, under free tropospheric conditions.

The concentration of these VOCs at MO are in the same order of magnitude as those reported in previous studies (Rocco et al., 2020; Verreyken et al., 2021). On the other hand, higher concentrations of benzene, methanol and acetone are measured at PF than at MO, indicating that the former site is located closer to emission sources. This induces that the range of the measured VOC concentrations is larger at PF compared to MO and therefore that the values of STD are larger. In comparison with B elouve measurements from OCTAVE (2018) (Rocco et al., 2020), concentrations of methanol and acetone are two times greater at PF suggesting that anthropogenic or marine sources can be a large contribution of these compounds at PF. Indeed (Colomb et al., 2009), show high concentrations of methanol and acetone in the marine boundary layer (Colomb et al., 2009;  $1.93 \pm 0.28$  ppbv and  $1.08 \pm 0.18$  ppbv, respectively). Residual concentrations of these compounds can be measured during the night and explain the higher concentrations at PF than B elouve.

Methanol and acetone show significant concentrations for both sites (until 5 ppb at PF and 2 ppb at MO, Figures 6c and 6d). Strong diurnal variations are observed for these compounds. A shift of 2 hr for methanol concentrations between the two sites shows that these compounds are not only formed or emitted at MO but are also advected from downhill. These compounds are emitted by primary and secondary ways by reaction of methyl peroxy radicals ( $\text{CH}_3\text{O}_2$ ) with other peroxy radicals for methanol (Madronich & Calvert, 1990; Tyndall et al., 2001) and formed by organic precursors such as hydrocarbons for acetone (Jacob et al., 2002).

Benzene is present at PF in higher concentrations (Figure 6e), probably due to a higher traffic density. Similar to methanol, this compound is advected toward MO during the day. Higher concentrations of benzene is observed while concentration under detection limit are often observed during the night. Advection from PF to MO is clearly demonstrated on April 3. Indeed, the peak of benzene of 0.1 ppb at PF is observed at 3 hr UT and can be seen 3 hr later at MO (0.05 ppb).

Surprisingly, the concentration of isoprene is in the same order of magnitude in both sites with the maximum concentration of 0.06 ppb (Figure 6a). Generally, on the diurnal variation, two peaks have been observed. The first peak is present in the morning and shows local emissions of this compound at both sites. At 5–6 hr UT, cloud formation is occurring (Lesou ef et al., 2013), and the concentration of isoprene decreases. This depletion can be

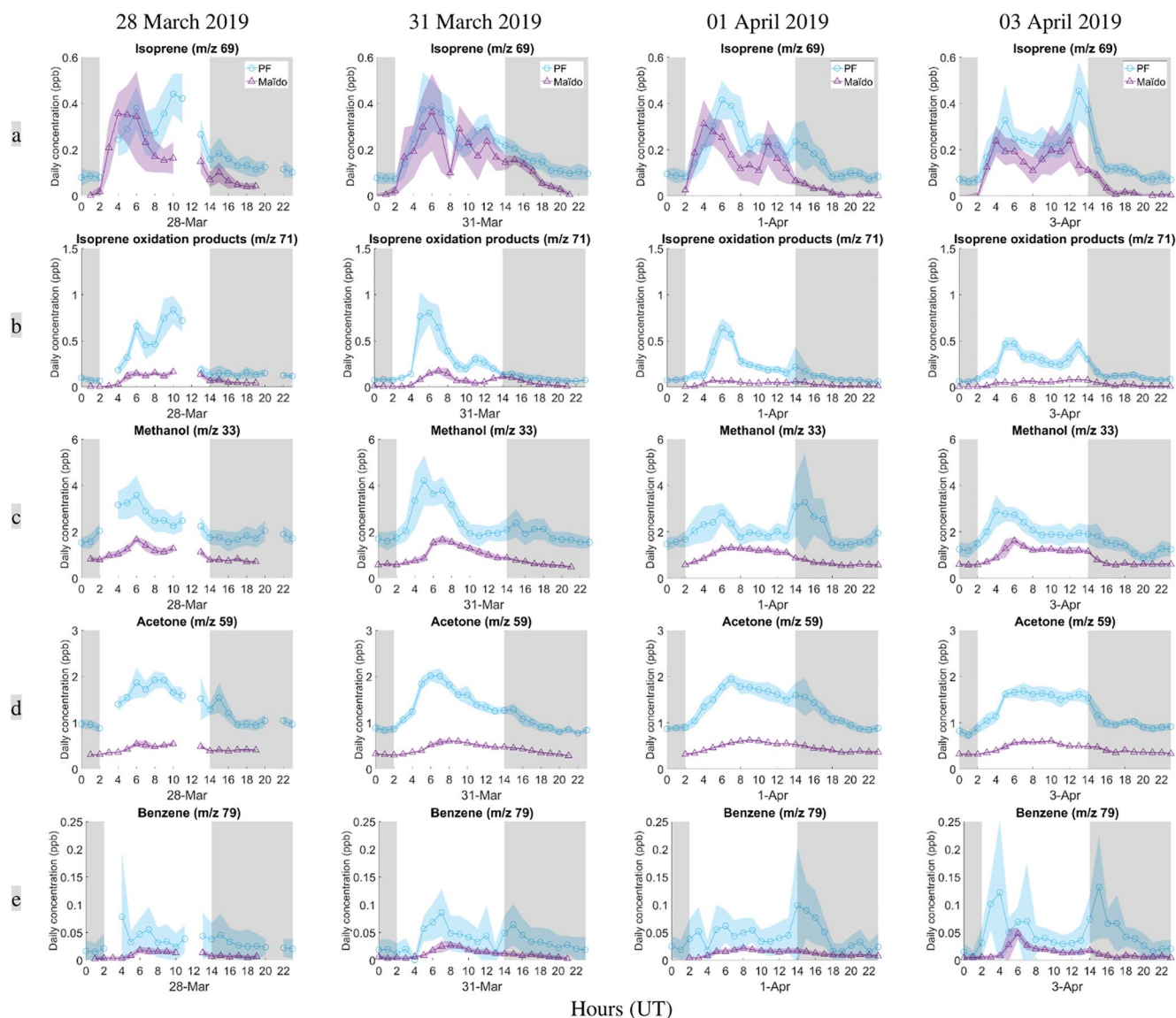


**Figure 6.** Concentration of volatile organic compounds (isoprene, isoprene oxidation products, methanol, acetone, and benzene) from March 31, 2019 to April 1, 2019, with average concentration during the night (20–23hr UT) in Petite France (blue) and at the Maïdo Observatory (purple).

mostly explained by the decrease of solar radiation and temperature, affecting the biogenic emission of isoprene (Monson et al., 1992; Rinne et al., 2002), and by the oxidation processes of this compound leading to consumption and decrease. A recent study had shown the presence of low-soluble VOCs, such as isoprene, in cloud water at Réunion Island (Dominutti et al., 2021). Even though the transfer from gas to the aqueous phase represents a minor sink due to isoprene’s solubility, this mechanism could also affect the depletion observed. Furthermore, the difference in  $\text{NO}_x$  concentration (Figure S2 in Supporting Information S1) could play a role in VOCs emission or formation and, then in calculated ratios. Isoprene emissions induce the formation of its oxidation products during the day. Oxidation seems very strong at PF in comparison to MO. Indeed, isoprene oxidation products present strong diurnal variation with significant concentration (up to 1 ppb) at PF.

Table 4 reports daytime and nighttime averaged ratios of VOCs concentrations between sites  $[C_{\text{MAÏDO}}]/[C_{\text{PF}}]$ . Daytime ratios have been calculated from 2 to 14 hr UT and then averaged for each day and nighttime ones from 14 to 2 hr UT. For this analysis only the days dynamically connected were considered.

**Table 3**

*Averaged Measured Concentrations During All Day (Day and Night Including) and During the Night (From 20 to 23 hr UT Except for March 28 for Which Night Mean Values Have Been Calculated From 2 to 4 hr UT Due to a Lack of Measurement at MO) and Their Standard Deviation at the MO and at PF Sites for March 28 and 31 and April 1 and 3, 2019*

Compounds	Site	Isoprene	Isoprene oxidation products	Methanol	Acetone	Benzene	$\sigma$
28/03/2019	PF	0.179 ± 0.114	0.207 ± 0.192	1.965 ± 0.779	1.238 ± 0.385	0.040 ± 0.041	1.15 ± 1.68
Day concentration ± std (ppb)	MO	0.221 ± 0.148	0.130 ± 0.107	1.087 ± 0.366	0.452 ± 0.101	0.014 ± 0.009	0.58 ± 0.73
Night concentration ± std (ppb)	PF	0.168 ± 0.103	0.159 ± 0.122	1.798 ± 0.685	1.175 ± 0.318	0.089 ± 0.042	
	MO	0.032 ± 0.064	0.022 ± 0.033	0.651 ± 0.162	0.346 ± 0.066	0.006 ± 0.005	
31/03/2019	PF	0.208 ± 0.115	0.240 ± 0.235	2.307 ± 0.861	1.298 ± 0.410	0.040 ± 0.035	1.15 ± 2.04
Day concentration ± std (ppb)	MO	0.203 ± 0.143	0.072 ± 0.062	1.105 ± 0.387	0.471 ± 0.112	0.014 ± 0.009	0.35 ± 0.43
Night concentration ± std (ppb)	PF	0.169 ± 0.105	0.165 ± 0.153	1.969 ± 0.826	1.255 ± 0.398	0.039 ± 0.040	
	MO	0.078 ± 0.061	0.048 ± 0.040	0.652 ± 0.129	0.377 ± 0.066	0.007 ± 0.005	
01/04/2019	PF	0.181 ± 0.107	0.179 ± 0.159	2.033 ± 0.860	1.309 ± 0.397	0.042 ± 0.042	0.98 ± 1.48
Day concentration ± std (ppb)	MO	0.178 ± 0.105	0.069 ± 0.021	1.137 ± 0.193	0.594 ± 0.067	0.016 ± 0.005	0.38 ± 0.20
Night concentration ± std (ppb)	PF	0.095 ± 0.028	0.070 ± 0.025	1.583 ± 0.285	0.859 ± 0.093	0.025 ± 0.020	
	MO	0.051 ± 0.080	0.023 ± 0.018	0.638 ± 0.101	0.387 ± 0.054	0.008 ± 0.004	
03/04/2019	PF	0.179 ± 0.121	0.202 ± 0.141	1.723 ± 0.582	1.216 ± 0.371	0.048 ± 0.050	1.13 ± 1.16
Day concentration ± std (ppb)	MO	0.175 ± 0.070	0.081 ± 0.022	1.211 ± 0.231	0.519 ± 0.070	0.019 ± 0.014	0.46 ± 0.32
Night concentration ± std (ppb)	PF	0.072 ± 0.025	0.078 ± 0.027	1.134 ± 0.323	0.862 ± 0.091	0.023 ± 0.018	
	MO	0.041 ± 0.054	0.023 ± 0.022	0.641 ± 0.095	0.371 ± 0.044	0.006 ± 0.004	

*Note.*  $\sigma$  represents the ratio of isoprene oxidation products and isoprene concentrations.

The first finding is that the calculated daytime ratio does not vary by more than 6% for isoprene, 3% for oxidation products of isoprene, 6% for methanol, 3% for acetone and 4% for benzene. It can be noted that the ratios are lower than 1 for all the days and nights, which indicates that VOC concentrations of studied compounds at PF are higher than those obtained at MO (Table 4). Also, it suggests that air masses between PF and MO have undergone either deposition-dilution processes or photochemical reactions leading to a decrease of VOC concentrations.

Methanol ratios are almost constant during the 4 days and nights observed. The methanol daytime ratio varies from  $0.45 \pm 0.07$  (March 28) to  $0.56 \pm 0.12$  (April 3) but given the standard deviations it remains at the same level. Likewise, the acetone ratio remains constant around 0.3 during this period. Even if these two compounds have a long lifetime in the atmosphere (12 days and 61 days, respectively; Atkinson & Arey, 2003), a ratio lower than 1 indicates that dilution, photochemical reactions and deposition of these compounds occur during the transport of

**Table 4**

*Estimation of Daytime (2–14 hr UT) and Nighttime (14–2 hr UT) Ratios  $[C_{MAIDO}]/[C_{PF}]$  (Mean ± Standard Deviation) for Each Selected Day*

Date (DD/MM/YY)	Compounds	Isoprene	Isoprene oxidation products	Methanol	Acetone	Benzene
28/03/2019	Daytime Ratio	0.68 ± 1.13	0.28 ± 0.32	0.44 ± 0.39	0.28 ± 0.26	0.27 ± 0.16
	Nighttime Ratio	0.32 ± 0.83	0.40 ± 0.77	0.44 ± 0.25	0.35 ± 0.20	0.19 ± 0.17
31/03/2019	Daytime Ratio	0.78 ± 1.18	0.29 ± 0.32	0.43 ± 0.40	0.31 ± 0.29	0.34 ± 0.25
	Nighttime Ratio	0.64 ± 1.16	0.73 ± 1.48	0.36 ± 0.28	0.40 ± 0.38	0.25 ± 0.18
01/04/2019	Daytime Ratio	0.77 ± 0.99	0.23 ± 0.18	0.51 ± 0.46	0.33 ± 0.32	0.32 ± 0.22
	Nighttime Ratio	0.17 ± 0.35	0.31 ± 0.29	0.33 ± 0.12	0.38 ± 0.23	0.28 ± 0.11
03/04/2019	Daytime Ratio	0.68 ± 0.72	0.24 ± 0.24	0.55 ± 0.55	0.34 ± 0.31	0.34 ± 0.27
	Nighttime Ratio	0.14 ± 0.38	0.19 ± 0.38	0.47 ± 0.32	0.37 ± 0.24	0.15 ± 0.10

the air masses. Dry and wet deposition of these compounds has been estimated to be 12% and 30% of total removal processes in the atmosphere for acetone and methanol, respectively (Heikes et al., 2002; Singh et al., 1994).

In the case of benzene ratios, an anthropogenic VOC (lifetime of 9 days, Atkinson, 2000), nighttime and daytime ratios are in the same order for all days ( $\sim 0.3$ ) with higher concentrations at PF than at MO. Benzene and acetone present the same ratio, suggesting the same dilution and/or deposition processes, whereas methanol has a larger ratio showing potential local sources from vegetation at MO. Ratio of inert gas such as carbon monoxide (CO) shows median ratio of 0.29 (0.21–0.43; 25–75 percentiles) from data sampling of the whole campaign and a median ratio of  $0.29 \pm 0.08$ ,  $0.26 \pm 0.12$ ,  $0.39 \pm 0.24$ , and  $0.24 \pm 0.11$ , for the four selected days. This indicates that processes of dilution and/or dry deposition are occurring between the two sites and even when air masses are not coming from PF.

Acetone shows a higher ratio at night than daytime, suggesting an additional acetone contribution during the day at PF which can originate from secondary products of VOC photo-oxidation, or brought by a local source. Furthermore, high residual concentrations of acetone have been observed during the night at PF which can explain these ratios.

Regarding biogenic VOC, during the daytime, isoprene average ratio is  $0.73 \pm 1.01$  and during nighttime  $0.32 \pm 0.68$  while isoprene oxidation products ratios are  $0.26 \pm 0.26$  (day) and  $0.41 \pm 0.73$  (night). The larger ratio of isoprene, which has a short lifetime (1.4 hr, Atkinson, 2000), indicates that there is an additional source of isoprene (local source) close to MO. Furthermore, the ratios between isoprene oxidation products and isoprene (named  $\sigma$ ) are presented in Table 3. Higher ratios have been observed at PF than MO, showing that oxidation processes are more significant in PF than MO as already underlined before. The  $\sigma$  ratio, if we are in a classic box model, must increase with time, because isoprene is consumed 3 times faster than MVK or MACR. But this ratio is lower at the MO and could be explained by two ways: loss of MVK + MACR by dissolution in the water of the cloud (1) and increase of the isoprene concentration on the way new fresh emission of isoprene close to the Mado (2).

In the next section, normalized concentrations ratios are presented to get an overview of the diurnal variation of the VOC enrichment during the day and their link with air masses trajectories and land cover footprint.

### 3.3. Normalized VOC Concentrations at PF and the MO and Their Link With Air Masses Trajectory and Land Cover Footprint

Average day and night concentrations (ppbv) for the selected VOC are reported in Table 4. VOC concentrations are in the same range as those obtained during the same period in 2018 (Rocco et al., 2020), and during a long-term observation campaign (Verreyken et al., 2021) at MO. Overall, higher concentrations of VOCs were observed during the day for both sites. Between the VOC, oxygenated species such as methanol and acetone (and HCHO not shown here) presented the highest mixing ratios (Table 4).

In order to analyze diurnal variations more precisely, normalized VOC concentration to night concentrations (concentration of compound X/average concentration of compound X from 20 to 23 hr UT) were calculated. Normalized concentrations plots have the advantage to better show the variation of concentration of VOCs during daytime for low concentrations as measured at MO and to enable to compare with those at PF. Figure 7 displays the diurnal variation of selected VOC at PF and MO. This kind of representation is used to evaluate the sinks or the contribution of VOC concentration during the day. A concentration above 1 indicates that the concentration increases during the day compared to the values during the night. Conversely, a concentration below 1 indicates that concentration during the night is higher than the concentration during the day and there is a depletion of VOCs (dilution, oxidation...).

The backward trajectories have been calculated in the 500 m resolution domain to determine the land cover footprint of air masses and their potential influence on measured VOC concentrations at the island scale (Figure 8). They start from MO every 15 min from March 15 to April 8, 2019. Thresholds of 500 m over the ground level are established to consider only the air masses which are most influenced by surface land cover footprint determined with the Corine Land Cover 2018 data interpolated on trajectory points. Most of the time points 1,000 m above ground level are above the mixed boundary layer and are less affected by the surface emissions. The trajectory points located above the altitude threshold are considered less influenced by the surface and are therefore

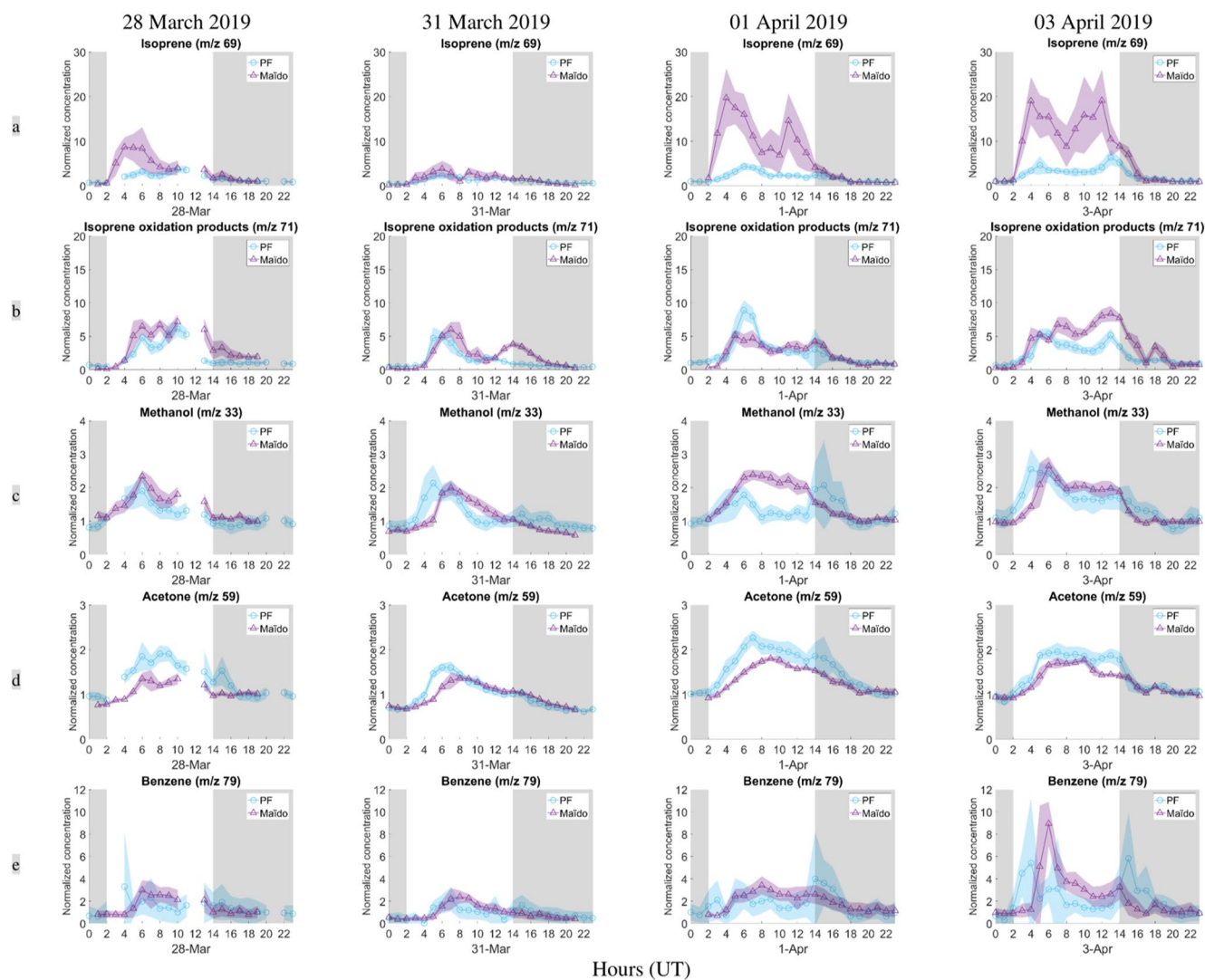


**Figure 7.** Normalized concentration of volatile organic compounds to average night concentration (isoprene (a), MACR + MVK (b), methanol (c), acetone (d), benzene (e)) for March 28, March 31, April 1, and April 3, 2019 at Petite France (blue) and Maïdo Observatory (purple). Average concentration during the night were obtained from 20 to 23 hr UT. Gray areas represent nighttime.

classified in a "high altitude" category. The daily percentages of category influences are given in Figure 8 for the altitude threshold. Backward and forward trajectories every 3 hr for the four chosen days are presented in the Supporting information (Figures S3, S4, S5, and S6 in Supporting Information S1).

### 3.3.1. Normalized VOC Concentrations at Petite France

During the four selected days, most compounds show their normalized concentrations higher than 1 at PF (Figure 7). Isoprene is well known to be most emitted during the day by biogenic sources which depend on temperature and light conditions (Monson et al., 1992). Therefore, isoprene oxidation products are also formed during the day. The high diurnal normalized to night concentrations of isoprene products (e.g., MACR + MVK) show that this oxidation process is very important at PF. Moreover, they are in the same order for the 4 days (Figure 6).

Methanol and acetone normalized to night concentration show a significant diurnal variation with maximal values between 5 and 18 hr UT (Figure 7, lines (c) and (d)). These compounds have anthropogenic, marine and biogenic origins (Bates et al., 2021; Heikes et al., 2002; Jacob et al., 2002, 2005; Wang et al., 2020). They can also be formed as secondary compounds (Jacob et al., 2002; Madronich & Calvert, 1990; Tyndall et al., 2001) and notably in biomass burning plumes (Holzinger et al., 2005).

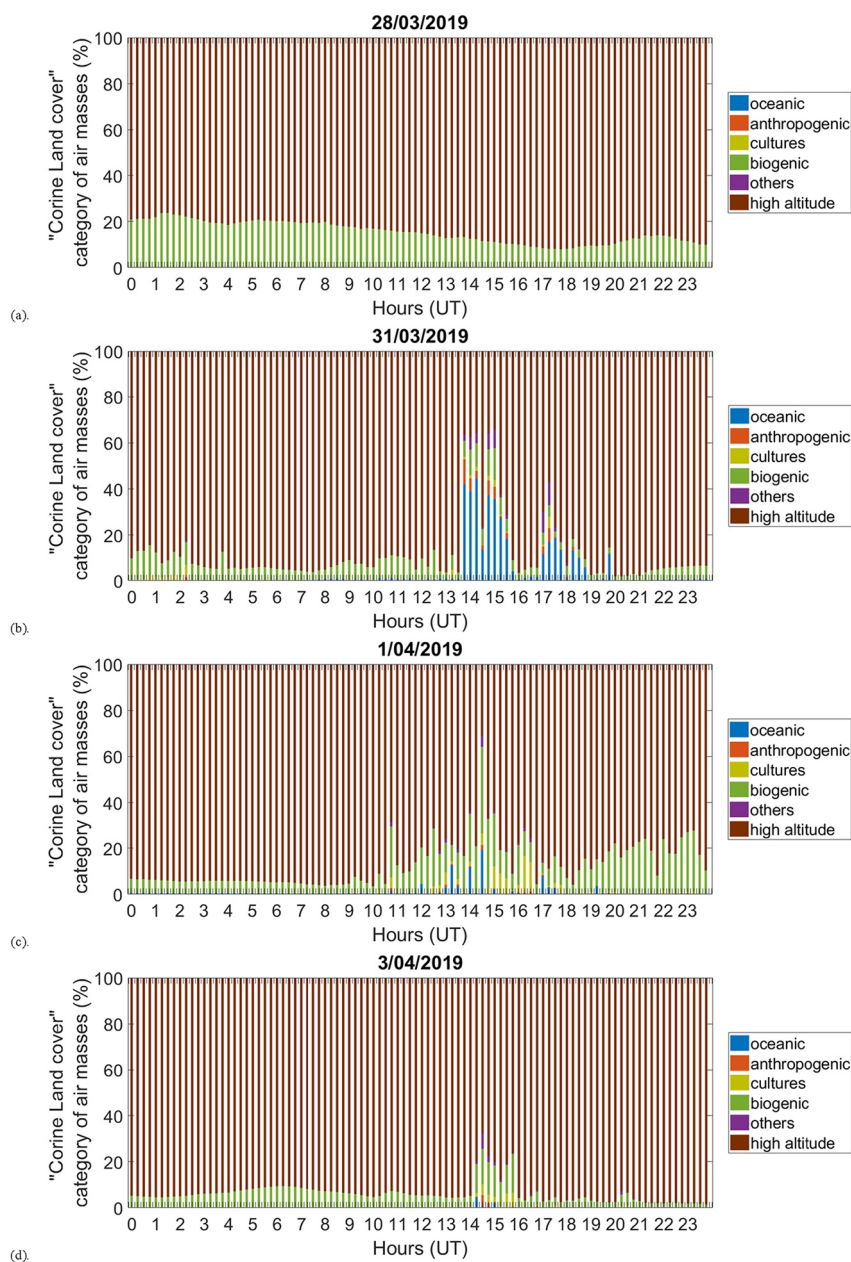


**Figure 8.** Corine Land cover categories of air masses (in %) for March 31, 2019 (a), March 28, 2019 (b), March 31, 2019 (c), April 1, 2019 and (d), April 3, 2019 calculated from 500 m backward trajectories every 15 min from the Maïdo observatory for points under 500 m. Six categories have been distinguished: oceanic (blue), anthropogenic (orange), cultures (light green), biogenic (dark green), others (purple) and high-altitude trajectories (brown).

No high normalized concentrations (such as observed for isoprene) have been observed for anthropogenic compounds (here benzene, Figure 7e) except on April 3, with two high peaks at 4 and 15 hr UT. The emissions of this compound are much localized and occur at specific moments (in the morning could be associated with traffic emissions) that explains the concentration spike during the day.

PF presents patterns of emissions associated with local sources during the day from biogenic and anthropogenic VOCs, but also by the secondary VOCs produced in the local atmosphere.



### 3.3.2. Normalized VOC Concentrations at the Maïdo Observatory and Link With the Corine Land Cover at the 500 m Domain

Unsurprisingly, higher normalized concentrations have been measured at MO during the day in comparison to PF, which means higher amplitude between day and night at MO than PF. Indeed, PF is always in the boundary layer (see residual concentrations during the night, Figure 6) whereas MO is located in the PBL during the day and in the free troposphere at nighttime. Significant normalized to night concentrations are observed of isoprene, isoprene oxidation products, acetone and methanol for the 4 days. A shift of about 2 hr in the maximum concentrations between measurements at PF and MO (Figure 7) can be observed for methanol and acetone for most of the days. High normalized concentration of methanol and acetone during daytime and nighttime for March 28 and 31 have been observed. These compounds have several origins such as biogenic and anthropogenic origin, and also an oceanic origins (Bates et al., 2021; Heikes et al., 2002; Millet et al., 2008; Singh et al., 1994; Wang et al., 2020). Significant anthropogenic (industrial and urban) influences can explain the notable concentration of benzene. For this compound, the normalized concentration is different at MO compared to PF. Acetone, methanol, and benzene normalized concentrations stays in the same order of magnitude for the four selected days (Figures 7c–7e).

On March 28, a high normalized concentration has been observed for isoprene and its products (up to 10 and 5, respectively, Figures 7a and 7b). Isoprene normalized concentration presents a high increase at 3hr UT that coincides with the sunrise and with the increase of temperature. The diurnal variation of isoprene shows the same pattern as the mountainous capped diel wind cycle with west wind from Verreyken et al. (2021) (calculated for the marine, urban, mountain and capped mountain categorical emission sources with FLEXPART-AROME 12-hr back trajectory calculations). The dilution of PBL leads to a decrease in normalized concentration after 13 hr UT. As suggested previously, the cloud formation induces a decrease of the intensity of solar radiation and then, isoprene emissions. Then, in a second step, it can induce a transfer of gas-phase VOCs into cloud droplets (Dominiutti et al., 2021). Indeed, isoprene is the major VOC present in cloud droplet (55.4% of total VOC measured). Most of backward trajectories from MO show that air masses come from southeast and high altitude. Regarding forward trajectories from PF, a lot of air trajectories showed that air masses are going to MO (Figure S3 in Supporting Information S1). Thus, VOC measured (a not particular case of isoprene which has been emitted locally) at MO have been likely advected from downhill to MO thanks to anabatic winds and sea-breeze phenomenon.

For this day (March 28), numerous masses are coming from altitude and southeast (Figure S3 in Supporting Information S1). This day shows no cases of dynamical connection between PF and MO from backward trajectories. Surprisingly, forward trajectories from PF on the same day show the connection between sites (Figure S3 in Supporting Information S1). A lot of trajectory points have been observed above 500 m (high altitude percentage category in Figure 7a). No clear diurnal variation has been observed but more trajectory points below the threshold have been observed during the night and a part of the day. This day presents a high biogenic footprint (20%) because meso-CAT indicates a significant residence time in the close vicinity of MO where the soil is classified as biogenic by the Corine Land Cover register (Figure 8a). As backward trajectories have been only selected, they do not explain benzene concentrations measured at MO. Nevertheless, PF forward trajectories show that air masses are starting from downhill and reaching the MO altitude, explaining the variations of concentration measured in MO.

On March 31 presents with several dynamical connections between PF and MO (Figure S4 in Supporting Information S1) but, surprisingly, it does not show greater normalized concentrations of isoprene and its products than the other days. It can be explained by the high oceanic and low biogenic origins of air masses during this day (Figure 8b). However, methanol and acetone present significant normalized concentration during the day that is in line with the oceanic origin measured with Corine Land Cover (Figure 8b). At 14 hr UT, the oceanic origin increases and becomes dominant reaching up to 55% when wind direction at MO becomes ENE (east-north-east). From 8 to 12hr UT, the slope toward MO is under the influence of up-slope winds and the sea-breeze phenomenon. Air masses come from the north and pass-through above Saint-Denis and canyons to join MO, bringing a little percentage of oceanic and anthropogenic origin (2% and 1%, respectively). During this period most air masses at PF are coming from downhill due to strong changes in wind regimes. At 13 hr UT, air masses come from the northwest and are influenced by the “Rivière des Galets” canyon (at the northwest of MO), passing over PF and reaching MO. At 14 hr UT, it is nighttime and the ground behind is cold inducing a change of wind regime with katabatic winds and land-breeze. But the wind system remains and brings oceanic air masses to MO.

From 14 to 19hr UT, more diversified influences are observed with biogenic, anthropogenic, and other origins (air masses passed through Le Port, a big industrial city in the northwest of the Réunion Island, along the coast). Traffic, urban, port and industrial areas represent few percentages of the map (under 10%). These areas represent a low surface compared to biogenic or cultivated areas which represent 59% and 11% of the map, respectively. Urban areas and roads represent small surface areas while still having an impact on the chemical composition of air masses, depending on the category. The real influence of traffic, urban, port, and industrial areas is probably underestimated with our approach due to the low surface areas of these sources in the register. It is therefore not possible to compare quantitatively the influence of one category to another. However, our approach allows to establish temporal evolution of the influence of the air masses' origins and to compare from one date to another.

The normalized concentration of benzene is significant with a large peak during this day with a maximum at 8hr UT and which starts at 4hr UT and reaches its lower level at 19hr UT. This result is well-linked with the origin of air masses calculated from backward trajectories which show that 3% of them passed over anthropogenic areas from 12 to 19hr UT (Figure 8b). If we follow the evolution of air masses, no concentration should be measured before 12hr UT. But the normalized concentration ratio shows an increase at 4hr UT that can be explained with mixed boundary layer effects. Indeed, as previously said, the boundary layer increases in altitude during the day and can bring compounds to the MO.

A lot of air masses are coming from the northwest of the mountain (Figure S4 in Supporting Information S1) on March 31. MO is under the influence of northerly winds. Between 3% and 34% (min% and max%), 0% and 17% and 0% and 14% of air masses passed over vegetation, cultures and anthropogenic areas, respectively (Figure 8b). Most of the time, air masses passed over vegetation and culture areas. MO is then influenced by highly biogenic areas around this site. Reunion Island is known for its sugar cane culture which covers 54% of the agricultural area. Other category origins ranged between 1% and 18% from 14 to 19hr UT.

On April 1, air masses are coming from the downhill of MO (Figure S5 in Supporting Information S1). It is consistent with a higher normalized ratio of short lifetime VOC, such as isoprene but also for a long lifetime such as benzene and methanol. Anthropogenic origin has been observed from 9 to 19 hr UT, in agreement with backward trajectories origins (up to 3% of anthropogenic area, Figure S5 in Supporting Information S1). From 0 to 9 hr UT, air masses come from high altitudes, with high biogenic, culture, and oceanic influences.

As shown in Figure 8c, the number of high-altitude points is significant (93% of total). This induces that trajectory points considered are close to MO where biogenic and cultivated areas are mostly present, and the biogenic influence ranges between 5% and 9%. Despite this, the normalized to night ratio of isoprene is exceeding those measured on the other three days (March 28 and 31, and April 3) partly explained by the low concentration of isoprene measured at night (Table 3). From 9 to 19 hr UT, air masses provided from the downhill of MO are characterized by a low increase of the percentage of anthropogenic, cultures and other areas and a low percentage of oceanic areas. After 19 hr UT, air masses are coming from the south-west and altitude, which explains the lack of oceanic and anthropogenic origins.

The April 3 presents the same pattern of normalized VOCs concentration as April 1, but with higher levels for benzene (Figure 7e). The reason for this higher concentration can be explained by probably a more intense anthropogenic activity or more air masses with anthropogenic origins. On April 3, the backward trajectories are from the west side of the island passing over urban areas (Figure S6 in Supporting Information S1). For this day, the pattern is well-linked with the mountainous uncapped diel wind cycle as described in Verreyken et al. (2021). The concentration of isoprene decreases between 4 and 10 hr UT due to the cloud formation and the dilution of the boundary layer. But the up-slope phenomenon remains, and the concentration increases again at 10 hr UT when the cloud disappears. At 14 hr UT, the sun goes down and the phenomenon reverses generating katabatic winds and returning MO in the free troposphere.

Furthermore, this day shows a larger contribution of isoprene oxidation products with two significant peaks formed by cloud formation or dilution of boundary layer discussed above.

From 0 to 14 hr UT, we found the same pattern as on March 28. Selected categories are around the Maïdo and present higher biogenic and cultures areas. At 14 hr, the meteorological context changes and brings air masses from low altitude that explained the low percentage of oceanic origin (3%). At 15 hr 30 UT, air masses come always from the southeast but make a loop over the west coast and the cities on this coast (Figure S6 in Supporting

Information S1) as shown in Figure 8d with 3% of anthropogenic origin. The loop remains until 21 hr UT and disappears after this hour with air masses coming from the southeast. The loop can be explained by the presence of wind from the northeast advected by the anabatic wind (forward trajectories from PF, Figure S6 in Supporting Information S1) that deviate from the initial flow from the southeast.

To summarize, during the 4 days, air masses origin ranges from 3% to 46% for biogenic areas, 1%–17% for cultures areas, 3%–14% for anthropogenic areas, 6%–55% for oceanic origin and 6%–18% for other areas.

The concentrations measured at MO are then well explained by the Meso-CAT plots which show that diurnal variations are due to the contribution of low altitude air masses, with VOCs being advected from below MO.

#### 4. Conclusion

In this paper we present a new dynamical analysis of VOC concentration measurements at Réunion Island based on backward and forward trajectory calculations initialized with 100–500 m resolution topography and wind fields. Our results aims to provide a better understanding of chemistry and dynamics along the slope toward the MO. To fulfill this objective, two sites located at different altitudes on the western coast of the island (MO and PF) were targeted for VOC and meteorological parameter measurements. Our analyses were focused on the four selected days: March 28 and 31 and April 1 and 3, 2019. Based on these high spatial resolution simulations we have characterized the breeze processes (sea/land) and the mountain winds (katabatic/anabatic) and their influence on VOC concentrations.

The backward trajectories have been coupled with the “Corine Land Cover” register to provide an estimation of the percentage of points over a different category of the surface. We saw that the major category contributions were the biogenic area (mixed forest) and the cultures area (sugar cane plantation for example) which ranged between 3% and 46% and between 1% and 17% for each area respectively. Furthermore, when air masses are coming from downhill, we showed a significant oceanic origin with maximal recorded percentage up to 50% between 10 and 20 hr UT. However, the surface of traffic and industrial areas represent very small surfaces of the island, and the influence of industries and road traffic could be much greater than what is estimated with our approach.

The variability of VOC in concentration along the slope has been analyzed. The origin of air masses depends on the targeted day and the analysis can be very different among days. To summarize:

1. On March 28, backward trajectories show that no air masses are coming from PF to MO. But, regarding the forward trajectories from PF, a lot of air masses are advected to MO showing up-slope winds during the day.
2. On March 31, this day was marked by a high oceanic air masses origin (up to 50%). The main origin of the air masses is from the north and downhill of MO, the air masses are advected by the “Rivière des Galets” canyon.
3. On April 1, air masses were coming from west and southwest. Air masses origins showed also oceanic origin with high concentrations of methanol and acetone. Isoprene and its oxidation products ratio concentration ( $\sigma$ ) from MO to PF are  $0.86 \pm 0.72$  and  $0.98 \pm 0.49$ , respectively showing less oxidation of the air masses between the sites. The lower ratio at MO shows that isoprene emissions are higher and less oxidation is occurring in this site than PF.
4. On April 3, high anthropogenic origin has been highlighted from the south-east that is well linked with the concentration of benzene. Indeed, April 3 shows the highest concentration of benzene in comparison with the other case studies.

This new and first approach combines cover land footprint and backward trajectories. It provides information on the nature of the ground-surface during the few days and hours before the air mass arrives at the sampling sites. More modeling exercises such as 3D chemistry transport, including biogenic and anthropogenic emission inventories, are necessary to better evaluate the processes of oxidation, deposition, occurring on VOCs during the air mass transport.

Also, further investigation on trajectories evolution and their link with chemical measurements is needed to better understand what happened between the two sites and which reactions or dynamics processes are involved in the variation of concentrations with time.

The use of model tools in the future can bring a better understanding of dynamical and chemical processes occurring on the island. For example, chemical models (CLEPS, Mouchel-Vallon et al., 2017) can be used to reproduce the air mass evolution conditions from the bottom of the slope to the MO and can provide a better understanding of multiphase processes and exchanges involved in the cloud formation.

These model approaches are included in the BIO-MAÏDO project and are currently in progress.

## Data Availability Statement

The PTR-MS data set at Maïdo has been made available publicly (Amelynck et al., 2021).

## Acknowledgments

This research received funding from the Agence Nationale de la Recherche (ANR-18-CE01-0013). The authors are thankful for all BIO-MAÏDO campaign participants and their implications in this project. Meso-NH simulations have been made on Météo-France supercomputer. Météo-France also provided meteorological wind data presented in this study. The authors gratefully acknowledge the NOAA Air Resources Laboratory (ARL) for the provision of the HYSPLIT transport and dispersion model and READY website (<https://www.ready.noaa.gov>) used in this publication, all the developers of the FLEXPART software (<https://www.flexpart.eu>) and the Institut National de l'Information Géographique et Forestière (IGN) for the provision of Corine Land Cover (<https://land.copernicus.eu/pan-european/corine-land-cover>). The deployment of the BIRS-IASB PTR-MS at the Maïdo observatory was supported by the Belgian Federal Science Policy Office (grant no. BR/175/A2/OCTAVE) and extra financial support was received from Horizon 2020 (ACTRIS-2, grant no. 654109).

## References

- Ahern, A. T., Robinson, E. S., Tkacik, D. S., Saleh, R., Hatch, L. E., Barsanti, K. C., et al. (2019). Production of secondary organic aerosol during aging of biomass burning smoke from fresh fuels and its relationship to VOC precursors. *Journal of Geophysical Research: Atmospheres*, *124*(6), 3583–3606. <https://doi.org/10.1029/2018JD029068>
- Amelynck, C., Schoon, N., & Verreyken, B. (2021). Long-term in situ (O) VOC measurements at the maïdo observatory (reunion is-land) [Data Set]. Royal Belgian Institute for Space Aeronomy (BIRA-IASB). <https://doi.org/10.18758/17021061>
- Andreae, M. O., & Rosenfeld, D. (2008). Aerosol-cloud-precipitation interactions. Part 1. The nature and sources of cloud-active aerosols. *Earth-Science Reviews*, *89*(1–2), 13–41. <https://doi.org/10.1016/j.earscirev.2008.03.001>
- Atkinson, R. (2000). Atmospheric chemistry of VOCs and NOx. *Atmospheric Environment*, *34*(12–14), 2063–2101. [https://doi.org/10.1016/S1352-2310\(99\)00460-4](https://doi.org/10.1016/S1352-2310(99)00460-4)
- Atkinson, R., & Arey, J. (2003). Gas-phase tropospheric chemistry of biogenic volatile organic compounds: A review. *Atmospheric Environment*, *37*, 197–219. [https://doi.org/10.1016/S1352-2310\(03\)00391-1](https://doi.org/10.1016/S1352-2310(03)00391-1)
- Baasandorj, M., Millet, D. B., Hu, L., Mitroo, D., & Williams, B. J. (2015). Measuring acetic and formic acid by proton-transfer-reaction mass spectrometry: sensitivity, humidity dependence, and quantifying interferences. *Atmospheric Measurement Techniques*, *8*(3), 1303–1321.
- Baray, J. L., Courcoux, Y., Keckhut, P., Portafaix, T., Tulet, P., Cammas, J. P., et al. (2013). Maïdo observatory: A new high-altitude station facility at reunion island (21 S, 55 E) for long-term atmospheric remote sensing and in situ measurements. *Atmospheric Measurement Techniques*, *6*(10), 2865–2877. <https://doi.org/10.5194/amt-6-2865-2013>
- Baray, J. L., Deguillaume, L., Colomb, A., Sellegri, K., Freney, E., Rose, C., et al. (2020). Cézéaux-aunat-opme-puy de Dôme: A multi-site for the long-term survey of the tropospheric composition and climate change. *Atmospheric Measurement Techniques*, *13*(6), 3413–3445. <https://doi.org/10.5194/amt-13-3413-2020>
- Bates, K. H., Jacob, D. J., Wang, S., Hornbrook, R. S., Apel, E. C., Kim, M. J., et al. (2021). The global budget of atmospheric methanol: New constraints on secondary, oceanic, and terrestrial sources. *Journal of Geophysical Research: Atmospheres*, *126*(4), e2020JD033439. <https://doi.org/10.1029/2020JD033439>
- Bezďek, A., & Sebera, J. (2013). Matlab script for 3D visualizing geodata on a rotating globe. *Computers & Geosciences*, *56*, 127–130. <https://doi.org/10.1016/j.cageo.2013.03.007>
- Blake, R. S., Monks, P. S., & Ellis, A. M. (2009). Proton-transfer reaction mass spectrometry. *Chemical Reviews*, *109*(3), 861–896. <https://doi.org/10.1021/cr800364q>
- Clain, G., Baray, J.-L., Delmas, R., Keckhut, P., & Cammas, J.-P. (2010). A lagrangian approach to analyse the tropospheric ozone climatology in the tropics: Climatology of stratosphere–troposphere exchange at reunion island. *Atmospheric Environment*, *44*(7), 968–975. <https://doi.org/10.1016/j.atmosenv.2009.08.048>
- Colomb, A., Gros, V., Alvain, S., Sarda-Estève, R., Bonsang, B., Moulin, C., et al. (2009). Variation of atmospheric volatile organic compounds over the Southern Indian Ocean (3049°S). *Environmental Chemistry*, *6*(1), 70–82. <https://doi.org/10.1071/EN08072>
- Davis, E. V., Rajeev, K., & Mishra, K. M. (2020). Effect of clouds on the diurnal evolution of the atmospheric boundary-layer height over a tropical coastal station. *Boundary-Layer Meteorology*, *175*, 135–152. <https://doi.org/10.1007/s10546-019-00497-6>
- Dominutti, P., Renard, P., Vaitilingom, M., Bianco, A., Baray, J.-L., Borbon, A., et al. (2021). Insights into tropical cloud chemistry at reunion island (Indian ocean): Results from BIO-maïdo campaign. *Atmospheric Chemistry and Physics*, <https://doi.org/10.5194/acp-2021-518>
- Duflot, V., Tulet, P., Flores, O., Barthe, C., Colomb, A., Deguillaume, L., et al. (2019). Preliminary results from the FARCE 2015 campaign: Multidisciplinary study of the forest-gas-aerosol-cloud system on the tropical island of la Réunion. *Atmospheric Chemistry and Physics*, *19*(16), 10591–10618. <https://doi.org/10.5194/acp-19-10591-2019>
- Foucart, B., Sellegri, K., Tulet, P., Rose, C., Metzger, J. M., & Picard, D. (2018). High occurrence of new particle formation events at the Maïdo high-altitude observatory (2150 m), Réunion (Indian Ocean). *Atmospheric Chemistry and Physics*, *18*(13), 9243–9261. <https://doi.org/10.5194/acp-18-9243-2018>
- Garratt, J. R. (1992). *The atmospheric boundary layer*. Cambridge University Press. Cambridge: Wiley. <https://doi.org/10.1002/joc.3370140113>
- Heikes, B. G., Chang, W., Pilson, M. E. Q., Swift, E., Singh, H. B., Guenther, A., et al. (2002). Atmospheric methanol budget and ocean implication. *Global Biogeochemical Cycles*, *16*(4), 8080–113. <https://doi.org/10.1029/2002gb001895>
- Holzinger, R., Acton, W. J. F., Bloss, W. J., Breitenlechner, M., Crilley, L. R., Dusanter, S., ... & Zaytsev, A. (2019). Validity and limitations of simple reaction kinetics to calculate concentrations of organic compounds from ion counts in PTR-MS. *Atmospheric measurement techniques*, *12*(11), 6193–6208.
- Holzinger, R., Williams, J., Salisbury, G., Klüpfel, T., de Reus, M., Traub, M., et al. (2005). Oxygenated compounds in aged biomass burning plumes over the Eastern Mediterranean: Evidence for strong secondary production of methanol and acetone. *Atmospheric Chemistry and Physics*, *5*(1), 39–46. <https://doi.org/10.5194/acp-5-39-2005>
- Jacob, D. J., Field, B. D., Jin, E. M., Bey, I., Li, Q., Logan, J. A., et al. (2002). Atmospheric budget of acetone. *Journal of Geophysical Research*, *107*. <https://doi.org/10.1029/2001jd000694>
- Jacob, D. J., Field, B. D., Li, Q., Blake, D. R., de Gouw, J., Warneke, C., et al. (2005). Global budget of methanol: Constraints from atmospheric observations. *Journal of Geophysical Research*, *110*, D08303. <https://doi.org/10.1029/2004JD005172>

- Kesselmeier, J., & Staudt, M. (1999). An overview on emission, physiology and Ecology.pdf. *Journal of Atmospheric Chemistry*, 33, 23–88. <https://doi.org/10.1023/A:1006127516791>
- Lac, C., Chaboureaud, J. P., Masson, V., Pinty, J. P., Tulet, P., Escobar, J., et al. (2018). Overview of the meso-NH model version 5.4 and its applications. *Geoscientific Model Development*, 11(5), 1929–1969. <https://doi.org/10.5194/gmd-11-1929-2018>
- Lafore, J. P., Stein, J., Asencio, N., Bougeault, P., Ducrocq, V., Duron, J., et al. (1998). The meso-NH atmospheric simulation system. Part I: Adiabatic formulation and control simulations. *Annales Geophysicae*, 16(1), 90–109. <https://doi.org/10.1007/s00585-997-0090-6>
- Lesouéf, D., Gheusi, F., Chazette, P., Delmas, R., & Sanak, J. (2013). Low tropospheric layers over reunion island in lidar-derived observations and a high-resolution model. *Boundary-Layer Meteorology*, 149(3), 425–453. <https://doi.org/10.1007/s10546-013-9851-9>
- Lesouéf, D., Gheusi, F., Delmas, R., & Escobar, J. (2011). Numerical simulations of local circulations and pollution transport over reunion island. *Annales Geophysicae*, 29(1), 53–69. <https://doi.org/10.5194/angeo-29-53-2011>
- Lindinger, W., Hansel, A., & Jordan, A. (1998). On-line monitoring of volatile organic compounds at pptv levels by means of proton-transfer-reaction mass spectrometry (PTR-MS) medical applications, food control and environmental research. *International Journal of Mass Spectrometry and Ion Processes*, 173(3), 191–241. [https://doi.org/10.1016/S0168-1176\(97\)00281-4](https://doi.org/10.1016/S0168-1176(97)00281-4)
- Madronich, S., & Calvert, J. G. (1990). Permutation reactions of organic peroxy radicals in the troposphere. *Journal of Geophysical Research*, 95(D5), 5697–5715. <https://doi.org/10.1029/JD095iD05p05697>
- Masson, V., Champeaux, J. L., Chauvin, F., Meriguet, C., & Lacaze, R. (2003). A global database of land surface parameters at 1-km resolution in meteorological and climate models. *Journal of Climate*, 16(9), 1261–1282. <https://doi.org/10.1175/1520-0442-16.9.1261>
- Mellouki, A., Wallington, T. J., & Chen, J. (2015). *Atmospheric chemistry of oxygenated volatile organic compounds: Impacts on air quality and climate*. <https://doi.org/10.1021/cr500549n>
- Millet, D. B., Jacob, D. J., Custer, T. G., De Gouw, J. A., Goldstein, A. H., Karl, T., et al. (2008). New constraints on terrestrial and oceanic sources of atmospheric methanol. *Atmospheric Chemistry and Physics*, 8(23), 6887–6905. <https://doi.org/10.5194/acp-8-6887-2008>
- Monson, R. K., Jaeger, C. H., Adams, W. W., Driggers, E. M., Silver, G. M., & Fall, R. (1992). Relationships among isoprene emission rate, photosynthesis, and isoprene synthase activity as influenced by temperature. *Plant Physiology*, 98(3), 1175–1180. <https://doi.org/10.1104/pp.98.3.1175>
- Monti, P., Fernando, H. J. S., Princevac, M., Chan, W. C., Kowalewski, T. A., & Pardyjak, E. R. (2002). Observations of flow and turbulence in the nocturnal boundary layer over a slope. *Journal of the Atmospheric Sciences*, 59(17), 25132–2534. [https://doi.org/10.1175/1520-0469\(2002\)059<2513:OOFATI>2.0.CO](https://doi.org/10.1175/1520-0469(2002)059<2513:OOFATI>2.0.CO)
- Mouchel-Vallon, C., Deguillaume, L., Monod, A., Perroux, H., Rose, C., Ghigo, G., et al. (2017). Cleps 1.0: A new protocol for cloud aqueous phase oxidation of VOC mechanisms. *Geoscientific Model Development*, 10(3), 1339–1362. <https://doi.org/10.5194/gmd-10-1339-2017>
- Pinty, J.-P., & Jabouille, P. (1998). A mixed-phase cloud parameterization for use in a mesoscale non-hydrostatic model: Simulations of a squall line and of orographic precipitation. *Proceedings of the AMS Conference on Cloud Physics*, 217–220.
- Renard, P., Bianco, A., Baray, J.-L., Bridoux, M., Delort, A.-M., & Deguillaume, L. (2020). Classification of clouds sampled at the Puy de Dôme station (France) based on chemical measurements and air mass history matrices. *Atmosphere*, 11(7), 732. <https://doi.org/10.3390/atmos11070732>
- Rinne, H. J. I., Guenther, A. B., Greenberg, J. P., & Harley, P. C. (2002). Isoprene and monoterpene fluxes measured above Amazonian rainforest and their dependence on light and temperature. *Atmospheric Environment*, 36(14), 2421–2426. [https://doi.org/10.1016/S1352-2310\(01\)00523-4](https://doi.org/10.1016/S1352-2310(01)00523-4)
- Rocco, M., Colomb, A., Baray, J.-L., Amelynck, C., Verreyken, B., Borbon, A., et al. (2020). Analysis of volatile organic compounds during the OCTAVE campaign: Sources and distributions of formaldehyde on reunion island. *Atmosphere*, 11(2), 140. <https://doi.org/10.3390/atmos11020140>
- Rolph, G., Stein, A., & Stunder, B. (2017). Real-time environmental applications and display system: Ready. *Environmental Modelling and Software*, 95, 210–228. <https://doi.org/10.1016/j.envsoft.2017.06.025>
- Rumchev, K., Brown, H., & Spickett, J. (2007). Volatile organic compounds: Do they present a risk to our health? *Reviews on Environmental Health*. <https://doi.org/10.1515/REVEH.2007.22.1.39>
- Seinfeld, J. H., & Pandis, S. N. (2016). *Atmospheric chemistry and physics: From air pollution to climate change*.
- Sillman, S. (2002). Some theoretical results concerning O<sub>3</sub>-NO<sub>x</sub>-VOC chemistry and NO<sub>x</sub>-VOC indicators. *Journal of Geophysical Research*, 107(D22), 4659. <https://doi.org/10.1029/2001JD001123>
- Singh, H. B., O'Hara, D., Herlth, D., Sachse, W., Blake, D. R., Bradshaw, J. D., et al. (1994). Acetone in the atmosphere: Distribution, sources, and sinks. *Journal of Geophysical Research*, 99(D11), 1805. <https://doi.org/10.1029/93jd00764>
- Stein, A. F., Draxler, R. R., Rolph, G. D., Stunder, B. J. B., Cohen, M. D., & Ngan, F. (2015). NOAA's hysplit atmospheric transport and dispersion modeling system. *Bulletin of the American Meteorological Society*. <https://doi.org/10.1175/BAMS-D-14-00110.1>
- Tyndall, G. S., Cox, R. A., Granier, C., Lesclaux, R., Moortgat, G. K., Pilling, M. J., et al. (2001). Atmospheric chemistry of small organic peroxy radicals. *Journal of Geophysical Research*, 106(D11), 12157–12182. <https://doi.org/10.1029/2000JD900746>
- VanReken, T. M., Ng, N. L., Flagan, R. C., & Seinfeld, J. H. (2005). Cloud condensation nucleus activation properties of biogenic secondary organic aerosol. *Journal of Geophysical Research*, 110(7), 1–9. <https://doi.org/10.1029/2004JD005465>
- Verreyken, B., Amelynck, C., Brioude, J., Müller, J. F., Schoon, N., Kumpp, N., et al. (2020). Characterisation of African biomass burning plumes and impacts on the atmospheric composition over the south-west Indian Ocean. *Atmospheric Chemistry and Physics*, 20(23), 14821–14845. <https://doi.org/10.5194/acp-20-14821-2020>
- Verreyken, B., Amelynck, C., Schoon, N., Müller, J.-F., Brioude, J., Kumpp, N., et al. (2021). Measurement report: Source apportionment of volatile organic compounds at the remote high-altitude Maïdo observatory. *Atmospheric Chemistry and Physics Discussions*, 1–37. <https://doi.org/10.5194/acp-2021-124>
- Verreyken, B., Brioude, J., & Evan, S. (2019). Development of turbulent scheme in the FLEXPART-AROME v1.2.1 Lagrangian particle dispersion model. *Geoscientific Model Development*, 12(10), 4245–4259. <https://doi.org/10.5194/gmd-12-4245-2019>
- Vigouroux, C., Stavrou, T., Whaley, C., Dils, B., Duflot, V., Hermans, C., et al. (2012). Atmospheric chemistry and physics FTIR time-series of biomass burning products (HCN, C<sub>2</sub>H<sub>6</sub>, C<sub>2</sub>H<sub>2</sub>, CH<sub>3</sub>OH, and HCOOH) at Reunion Island (21 S, 55 E) and comparisons with model data. *Atmospheric Chemistry and Physics*, 12, 10367–10385. <https://doi.org/10.5194/acp-12-10367-2012>
- Wang, S., Apel, E. C., Schwantes, R. H., Bates, K. H., Jacob, D. J., Fischer, E. v., et al. (2020). Global atmospheric budget of acetone: Air-sea exchange and the contribution to hydroxyl radicals. *Journal of Geophysical Research: Atmospheres*, 125(15), e2020JD032553. <https://doi.org/10.1029/2020JD032553>
- Ylisirniö, A., Buchholz, A., Mohr, C., Li, Z., Barreira, L., Lambe, A., et al. (2020). Composition and volatility of secondary organic aerosol (SOA) formed from oxidation of real tree emissions compared to simplified volatile organic compound (VOC) systems. *Atmospheric Chemistry and Physics*, 20(9), 5629–5644. <https://doi.org/10.5194/acp-20-5629-2020>